ADVANCED ENERGY MATERIALS
www.advenergymat.de

Lithium Batteries and the Solid Electrolyte Interphase (SEI)—Progress and Outlook

Henry Adenusi, Gregory A. Chass, Stefano Passerini, Kun V. Tian, and Guanhua Chen**

Interfacial dynamics within chemical systems such as electron and ion transport processes have relevance in the rational optimization of electrochemical energy storage materials and devices. Evolving the understanding of fundamental electrochemistry at interfaces would also help in the understanding of relevant phenomena in biological, microbial, pharmaceutical, electronic, and photonic systems. In lithium-ion batteries, the electrochemical instability of the electrolyte and its ensuing reactive decomposition proceeds at the anode surface within the Helmholtz double layer resulting in a buildup of the reductive products, forming the solid electrolyte interphase (SEI). This review summarizes relevant aspects of the SEI including formation, composition, dynamic structure, and reaction mechanisms, focusing primarily on the graphite anode with insights into the lithium metal anode. Furthermore, the influence of the electrolyte and electrode materials on SEI structure and properties is discussed. An update is also presented on state-of-the-art approaches to quantitatively characterize the structure and changing properties of the SEI. Lastly, a framework evaluating the standing problems and future research directions including feasible computational, machine learning, and experimental approaches are outlined.

1. Introduction

The ever more pervasive technological advancements in modern society, industry, manufacturing, and agriculture, as well as those being implemented in solving global challenges remain accompanied by an energy reliance on non-renewable fossil fuels. The accelerated depletion of stocks of these energy sources, together with their associated pollution drives the need to expedite establishment of robust renewable alternatives. Often termed "renewables" or "clean energy," these power sources have a perennial temporal-availability and thus have greater need for energy repositories than non-renewables. Hence, prompt optimization of energy storage-delivery devices is crucial to the sustainable development, scaling, commercial delivery, and global establishment of reliable clean energy.[1,2]

Batteries and electrochemical devices have most often filled the majority of power-storage and are ubiquitous as energy mediation devices, capable of harnessing large amount of energy for various applications including the aerospace, travel and transport, and electronics industries, among others.[3–6] The future of batteries lies with devices produced from ever-more sustainable components that can offer improved safety, transportability, extended battery life, have short recharge times as well as low production costs and

H. Adenusi, G. Chen
Hong Kong Quantum AI Lab
17 Science Park West Avenue, Hong Kong, China
E-mail: ghc@everest.hku.hk

G. A. Chass
Department of Chemistry
School of Physical and Chemical Sciences
Queen Mary University of London
London E1 4NS, UK

G. A. Chass, K. V. Tian
Department of Chemistry and Biological Chemistry
McMaster University
Hamilton L8S 4L8, Canada
E-mail: kun.tian@uniroma1.it

The ORCID identification number(s) for the author(s) of this article can be found under https://doi.org/10.1002/aenm.202203307.

DOI: 10.1002/aenm.202203307

G. A. Chass, K. V. Tian
Faculty of Land and Food Systems
The University of British Columbia
Vancouver V6T 1Z4, Canada

S. Passerini
Department of Chemistry
Sapienza University of Rome
Rome 00185, Italy

S. Passerini
Helmholtz Institute Ulm
Helmholtzstrasse 11, 89081 Ulm, Germany

S. Passerini
Karlsruhe Institute of Technology
P.O. Box 3640, D-76021 Karlsruhe, Germany

K. V. Tian
Department of Chemistry and Chemical sciences of Pharmacy
Sapienza University of Rome
Rome 00185, Italy

G. Chen
Department of Chemistry
The University of Hong Kong
Hong Kong, China

good recyclability,[7–13] which together with carbon utilization (e.g., mineralization and carbonation) offer potential solutions to reducing atmospheric carbon.

Lithium-ion batteries (LIBs), which use lithium cobalt oxide $LiCoO_2$, lithium nickel cobalt manganese oxide, lithium nickel cobalt aluminum oxide or lithium iron phosphate $LiFePO_4$ as the positive electrode (cathode) and graphite as the negative electrode (anode), have dominated the commercial battery market since their introduction in the 1990s.[14–16] LIBs possess the highest gravimetric and volumetric energy-density amongst current commercially viable battery systems, hence they have been widely implemented in portable electronics, such as mobile phones, where space and weight limitations are paramount.[17,18] Recently, the use of LIBs has also risen in the automotive industry due to the increased production and proliferation of electric vehicles which are predicted to lead the overall mass market in the near future.[19] However, the application of LIBs is restricted by poor performance in varying climates (especially extreme cold), limited cycle life, liquid electrolyte safety risks (gas generation, leakage, fire, and even explosion), poor transportability, and high cost as well as finite lithium reserves.[20–22] These factors are underpinned by the role of the electrolyte, which modulates the primary function of the LIBs in terms of performance, operative lifetime, and safety.[23]

The developmental history of their predecessor lithium metal batteries (LMBs) is far more extensive, though their commercialization has been hampered primarily by safety issues,[24,25] in particular with respect to the dendritic and mossy metal deposits on the working lithium metal anodes which can cause internal short circuiting, triggering fires as well as explosions.[26] Further, the lithium dendrite formation on the interfacial layer between electrolyte and anode can significantly reduce the Coulombic efficiency. In contrast to the intercalation chemistry of LIBs, LMBs also suffer from stability (and cyclability) problems. Alternative cathode materials, such as oxygen and sulfur utilized in lithium-oxygen and lithium-sulfur batteries respectively, are unstable[27,28] and due to the low standard electrode potential of Li/Li^+ (−3.040 V versus 0 V for standard hydrogen electrode), nearly all lithium metal can be consumed during cycling and almost no electrolyte remains thermodynamically stable against metallic lithium.[25] As a result, LMBs possess inferior cycle life and safety profiles with respect to LIBs.[29–32]

The electrode/electrolyte interface is an important electrochemical juncture where reactions proceed involving lithium ions and electrons.[33] To achieve high energy densities, the electrodes in LIBs are designed to function at extreme potentials, thus electrolytes must operate beyond their thermodynamic stability limits.[34] The kinetic stability of electrolytes is attained when trace amounts decompose to form the solid electrolyte interphase (SEI) (**Figure 1**). The SEI is a complex heterogeneous structurally-disordered passivation layer that forms in situ, on the negative electrode.[35–39] SEI generation is essential for LIBs to reversibly charge and discharge, effectively enabling long-term cycling, a necessity for numerous applications, especially for electric vehicles.[40–45] Importantly, this interphase layer functions to inhibit further electrolyte degradation while facilitating lithium-ion transport through the layer onto the negative electrode.[46]

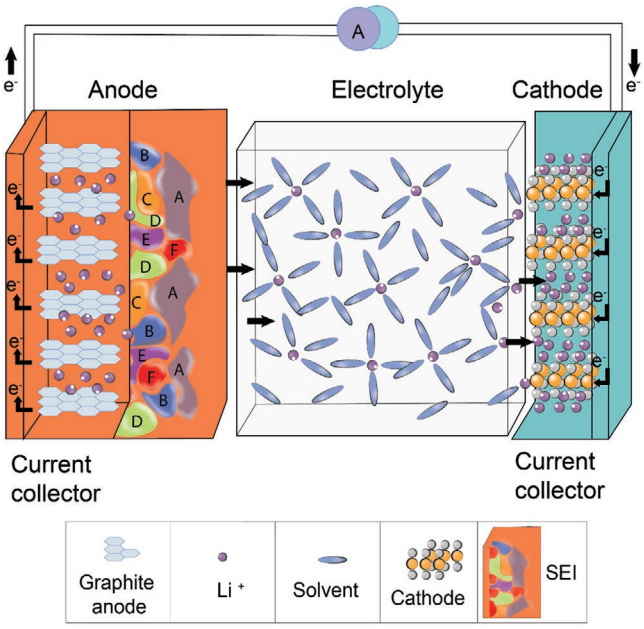

Figure 1. Schematic of a conventional LIB detailing the SEI layer with a snapshot of the initial SEI structure formed on graphite electrode interface which is primarily composed of lithium ethylene dicarbonate (LEDC) and lithium fluoride (LiF).

However, despite extensive research over the past three decades, the exact formation, composition, and functional mechanisms of the SEI remain one of the most ambiguous issues in battery science.[40] This is due to the spatially and temporally dynamic nature of this interfacial layer which forms during the initial charging process and grows in thickness over time as well as the changing surface mechanisms due to the continual reactions forming a complex, structurally-disordered polydispersive mixture.[47] What is known is that the SEI, being ≈10–50 nm thick, contains electrolyte decomposition products including both organic and inorganic species. Typically, the multi-layered SEI consists of an organic outer layer which is heterogeneous, porous, and permeable to both Li^+ and electrolyte solvent species at the SEI/electrolyte interface, while the inorganic inner layer near the electrode/SEI interface allows Li^+ transport.[43] SEI formation is highly influenced by the reactivity of the electrodes with the electrolytes.[37,43] A complete and stable SEI can restrict electron tunneling and prevent electrolyte reduction toward maintaining (electro)chemical stability of the battery, whereas an evolving SEI can continually consume electrolytes along with active lithium ions inducing increased battery resistance, capacity fading, and poor power density,[40,42,48] eventually promoting thermal runaway events leading to battery failure.[49–53]

In the first few battery charge cycles, graphite undergoes a limited volume change that slightly damages the SEI, expediting the loss of lithium. Such volume changes are prominent in the next-generation high-capacity anode materials such as silicon as well as lithium metal.[54,55] Additionally, the SEI layer on lithium metal is typically unstable and poorly understood with the relative volume change of lithium metal being effectively infinite. Further, the presence of dendrites widely detected in LMBs is a core challenge for characterization of the SEI on lithium metal

anode. To construct superior and safer batteries, a fundamental description of the SEI at the molecular level and its interfacial chemistry over extended time domains is requisite.

This review summarizes SEI formation, composition, and reaction mechanisms pertinent to this intricate layer, with foci primarily on the graphite anode with insights into the lithium metal anode. Furthermore, a discussion on the influence of electrolyte and electrode materials is provided along with a recap of the state-of-the-art approaches to investigate and characterize the SEI. Lastly, a framework evaluating the standing problems and future research directions including feasible computational, machine learning (ML), and experimental approaches are outlined.

2. A Brief History

The electrical properties of charged interfaces are affected by the characteristics of specific electrolyte ions in aqueous solutions. It has been established that both the surface charge densities and the electrical potentials depend on the species (solvents, salts, additives, etc.) present in the electrolyte solution.[56–59] These standard observations are known as specific ion effects, though the exact microscopic origins of these effects are complex thus driving research directions.[60,61] The concept of the electrical double layer (EDL) was first proposed by Helmholtz who suggested that a charged surface immersed in an electrolyte solution repels ions of like charges yet attracts their counterions.[62] The EDL consists of a layer of electronic charges at the electrode surface and a layer of counterions in the electrolyte, separated by a small distance (*H*) (**Figure 2**a).[63,64]

The Helmholtz model was revised by Gouy and Chapman (Figure 2b) who concluded that ions are mobile in the electrolyte solution and thus their distribution should be continuous, following the Boltzmann distribution.[65,66] This model accounts for the combined effects of the electrostatic forces considered in the Helmholtz model and the ion diffusion driven by concentration gradients caused by the electrical potential gradients (i.e., the electric field). The oppositely charged ions with respect to the electrode are distributed in an area of thickness greater than *H*. Nevertheless, the Gouy-Chapman model overestimates the EDL capacitance as it treats ions as point-charges leading to predictions of unrealistically elevated ion concentrations at the electrode surface.[63]

In 1924, Stern merged the Helmholtz and Gouy–Chapman models to explicitly define the Stern layer, the inner region of *H* (Figure 2c).[67] In the diffuse layer, the Gouy–Chapman model applies whereby the ions are mobile under the coupled influence of electrostatic forces and ion diffusion.

The presence of charged interfaces in batteries has now been correlated with the electrolyte structure within EDL, especially ion arrangements in the Stern layer.[68–71] Initially, before the inception of the SEI model, the Butler–Volmer equation was assumed, in which direct electron transfer from electrode to lithium cations in the solution ensued.[75] However, this was later proved incorrect because the electron transfer from the electrode to the electrolyte causes rapid self-discharge in the active materials. The first observation of the passivation layer was made by Dey in the 1970s.[72,73] Peled in 1979 first introduced the now widely accepted SEI model, applicable for all alkali metals and alkaline earth metals in non-aqueous battery systems.[74] Soon after, Peled proposed a double-layer SEI structure which is composed of a thin compact layer near the electrode and a thick and porous secondary layer near the electrolyte.[75] The first compositional information was determined by Nazri and Muller who detected the presence of lithium carbonate (Li_2CO_3) and oligomers on lithium surfaces.[76,77] Later, Aurbach et al. discovered lithium alkyl carbonates, in addition to Li_2CO_3 formed due to solvent decomposition.[78]

The formation of the passivation film on graphite was confirmed in 1990 by Fong et al.[79] Additionally, Kanamura et al. discovered that the compact layer near the lithium surface was

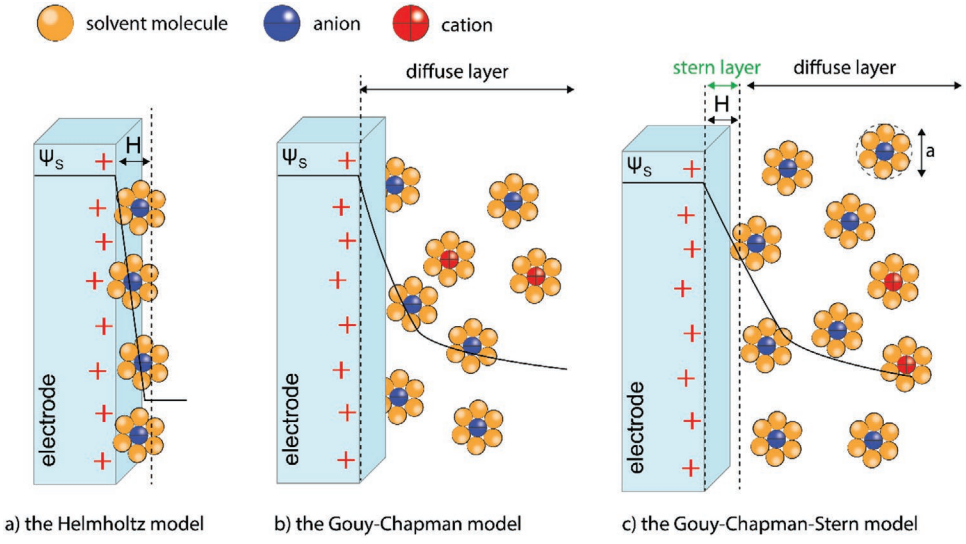

Figure 2. Representation of the electrical double layer structures as proposed by a) the Helmholtz model; b) the Gouy–Chapman model and c) the Gouy–Chapman–Stern model. H is the double layer distance in the Helmholtz model and Stern layer thickness; Ψ_s is the potential at the electrode surface. Inspired by Pilon et al.[70]

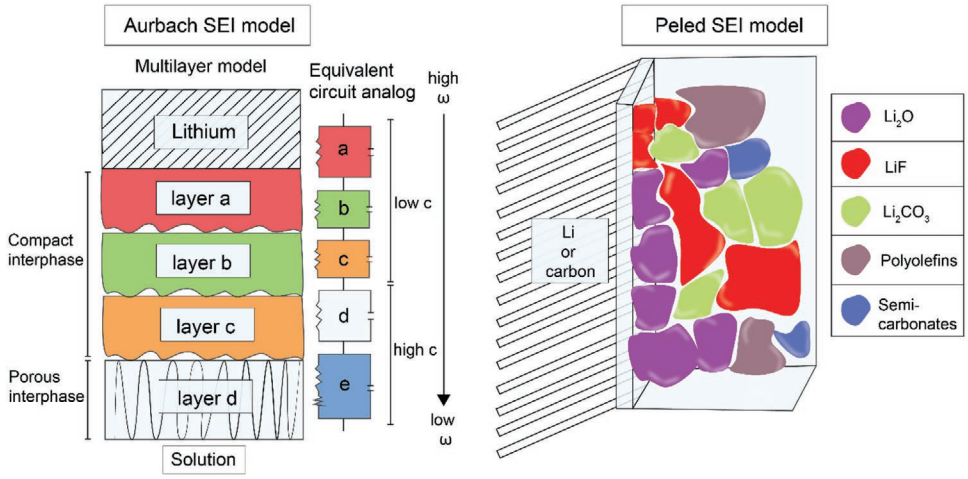

Figure 3. Schematic of the multilayer model on lithium electrode introduced by Aurbach et al. and the "mosaic" disordered poly-heterogenous microphase SEI model on lithium or carbon electrode as proposed by Peled et al.[82–84]

comprised of lithium fluoride (LiF) and lithium oxide (Li_2O), with the porous layer above this consisting of LiF along with organic compounds.[80,81] These led to Aurbach's multilayer model of the Li-solution interphase, highlighting the division of the various layers (**Figure 3**).[82] Peled et al. amalgamated previous results into the widely accepted "mosaic structure" of the SEI (Figure 3),[83,84] wherein the SEI is composed of both organic and inorganic products from electrolyte decomposition: specifically near the lithium surface, compact layers of inorganic species such as Li_2CO_3, LiF and Li_2O are thermodynamically stable against lithium,[78,80,84] whereas, near the electrolyte, the layers consist primarily of organic species like polyolefins and semicarbonates.[78,80,84] In 1999, Aurbach et al. illustrated the SEI formation processes commencing from electrolyte reduction on electrode surfaces.[85] Since the turn of the last century, further evidence of the multi-layered SEI on lithium and graphite electrodes was substantiated by Edström as well as Cresce et al. using in situ and synchrotron techniques.[35,86]

3. Current Progress

3.1. Electrochemical Stability of Battery Electrolytes

Advances in understanding the electrode/electrolyte interface stem from thermodynamic considerations of electrolyte reactivity in terms of reduction and oxidation at positive and negative potentials.[8,36,43,87] The widely accepted concept first introduced by Goodenough and Kim states that the SEI layer forms when the redox potential of the electrodes in a battery lies outside of the electrolyte electrochemical window. In this case, the stability window of a battery electrolyte is represented with the energy levels of the highest occupied molecular orbital (HOMO) and the lowest unoccupied molecular orbital (LUMO) of the solvent molecules. This concept of where electrolyte redox reactions take place is prevalent in the battery literature defining that at electron energies higher than the LUMO, the solvent-electrolyte is reduced, and at electron energy levels lower than the HOMO, the solvent-electrolyte is oxidized.[88–90] Electrolyte stability is further complicated by the fact that the electrolyte is a multi-component system consisting of solvents, salts, and additives, engaging in a myriad of interactions with the electrode surfaces, the strength, and nature of which are determined by configurational and conformational arrangements of the components.[71,91–95]

The HOMO-LUMO energy level is derived from approximated electronic structure theory exploring electronic properties of isolated species, hence their energy levels are not indicative of molecules participating in redox reactions. It has been established that the redox potentials are directly related to the Gibbs free energy difference between the reactants and reaction products. However, it is essential to understand that using such concepts alone can lead to erroneous descriptions.[43,92] For example, the calculated HOMO energies of battery solvents have led to overestimation of electrolyte stability neglecting H- and F-transfer reactions arising from electrolyte decomposition; the presence of other species also impacts the redox potentials of solvents, which may lead to an offset as high as 4 eV from the HOMO energies.[68,96] This is exemplified by the oxidation of isolated ethylene carbonate (EC) which occurs at ≈2 V higher and its HOMO energies ≈4 eV lower than the energy levels where the oxidation of the solvent transpires.[97] Thus, Peljo and Girault suggested that it is more correct to define the electrochemical stability of electrolytes as the potential of electrolyte reduction at negative potentials and the potential of solvent oxidation at positive potentials (**Figure 4**).[92]

The development of superior battery chemistry depends on the stabilization of electrode/electrolyte interfaces; recent quantum chemical (QC) electronic structure calculations highlight the influence of electrolyte redox stability.[71,98,99] This is governed by solvent-salt partitioning within the EDL near the electrolytes as well as the number of lithium cations complexing the solvents or anions (Figure 4). Consequently, these intricate phenomena impact the SEI formation and its structure and properties, which are further complicated by the coupling of electronic and ionic degrees of freedom in the layer. To a certain extent, the electronic insulation capability of the SEI components that can be quantified by the LUMO-HOMO gap may aid the understanding of the structure-property relationship at

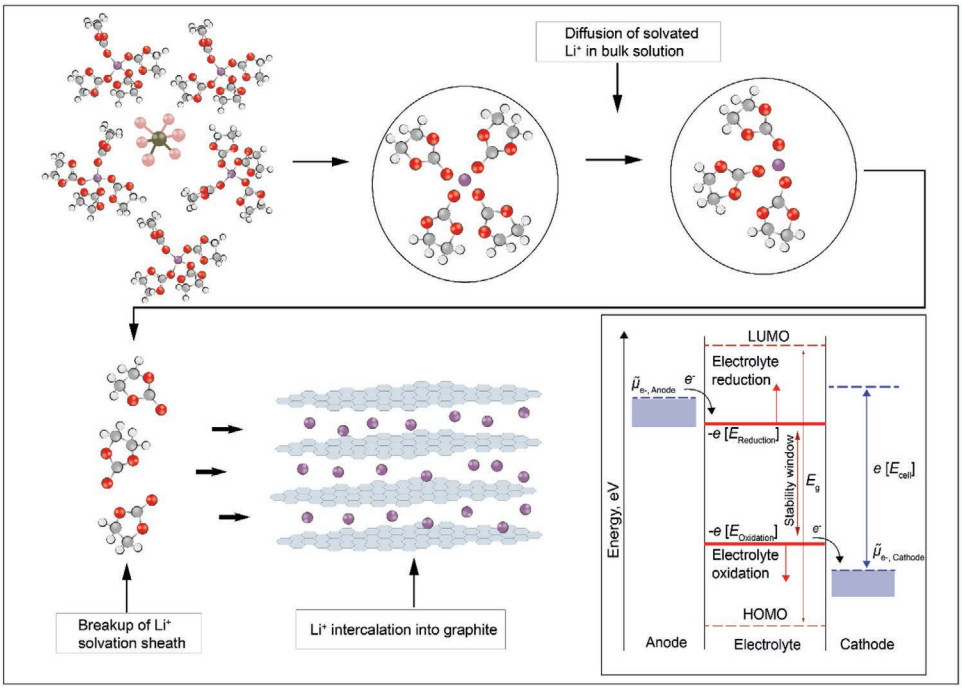

Figure 4. (Top) Example of interfacial electrolyte structure as solvated Li (in this example Li is coordinated to EC in the presence of PF_6 anion) diffuses and intercalates on the anode surface. The multi-component nature of the electrolyte highlights the complexity of the electrode/electrolyte interface in terms of electrochemical stability, structure, and dynamics. (Bottom) Electrochemical stability window of battery electrolytes; inspired by Peljo and Girault.[92]

the interface.[98] Such insights provide the foundation for the establishment of guiding principles for interphase formation.

3.2. SEI Formation, Composition, and Structure

The formation of the SEI is influenced by the cathode and anode materials along with the electrolyte composition.[46,100,101] The SEI formation completes under fast kinetics prior to the onset of the intercalation reaction, provided that the decomposition reaction potentials for the SEI formation are more positive than the anode lithium ion intercalation potential.[41] Most high purity electrolyte solvents have a decomposition potential of 4.6–4.9 V versus Li/Li^+, close to the preferred potential of 5 V for LIBs.[102] A complete SEI should possess high lithium-ion conductivity and negligible electronic conductivity to limit further reduction of the electrolyte on the graphite surface.[41] Whereas the ion conductive property facilitates the permeation of lithium ions, offering a pathway for ion intercalation in the graphite layers. Ideally, the SEI layer should be strong and flexible enough to withstand volume change due to expansion during charging and contraction during discharging of the anode throughout the cycling process.

To reduce the loss of irreversible capacity and lithium in the initial cycles, the SEI chemical composition should be comprised of stable, insoluble, and compact compounds, as the solubility of the decomposed SEI components is a key physical property for electrolytes to ensure a high-capacity retention. Studies on the heat of salt dissolution in EC:DMC (ethylene carbonate: dimethyl carbonate) have highlighted that inorganic compounds such as Li_2CO_3 are endothermic and hard to dissolve at normal operating temperatures.[103] While organic SEI components such as ROLi or $ROCO_2Li$ (R = alkyl group with a low molecular weight)[104] are among the most soluble compounds and the presence of such moieties can cause the diffusion of inorganic products into the electrolyte. Thus, an SEI containing Li_2CO_3 is preferred over one containing metastable organic species, such as ROLi or $ROCO_2Li$.

Dahn et al. first demonstrated that the lithium ions intercalate reversibly on graphitic carbon in liquid electrolytes that contains EC, due to the generation of the SEI,[79] and when propylene carbonate (PC) is utilized, irreversible lithium intercalation ensues, relevant to graphite exfoliation. Influentially, the difference of a single methyl group between EC and PC significantly alters the SEI composition and thus the effects of these distinctions have been the focus of numerous studies.[40,98,105,106] This highlights the importance and chemical specificity of the generated SEI which is regulated by its electrolyte precursor constituents as well as the resultant reactivity. The SEI formation on graphite in the presence of EC is highly stable, consisting predominantly of LEDC ($(CH_2OCO_2Li)_2$).[104,107–110] The morphological evolution of the SEI has been further elucidated with scanning electron microscopy (SEM),[49,111,112] suggesting that the SEI in the initial formation stages is comprised of loosely bound organic polymers, in contrast to the more compact inorganic salt structures as the potential decreased.

Further, the chemical composition, structure, and thickness of the SEI are also affected by the electrode surfaces.[113,114] A study by Zane et al. highlights the dependence of electrode performances on their surface chemistry in solutions.[113] The SEI morphology was altered with differing cycle times and temperatures (**Figure 5**). In addition, differences also arise between layers

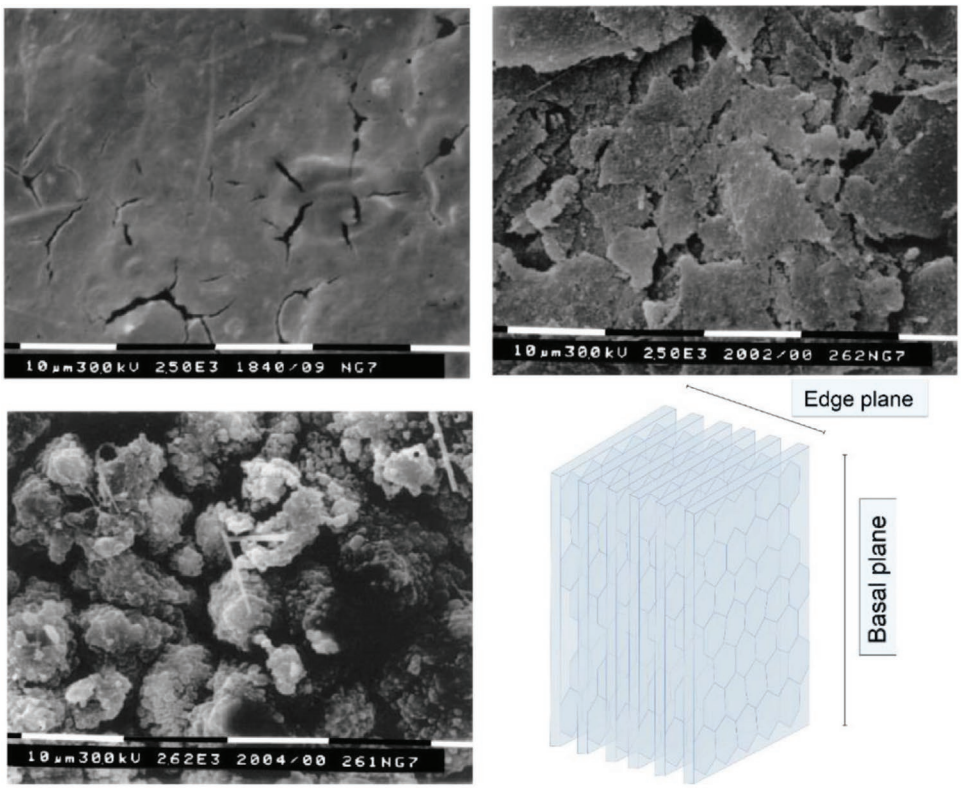

Figure 5. SEM micrographs (≈50 µm × 50 µm) of a surface SEI film on a graphite electrode in $LiBF_4$ EC/PC 3/1 solution: a) after the first discharge; b) after prolonged cycling at room temperature; c) after cycling at $T = 55$ °C. Reproduced with permission.[113] Copyright 2001, Elsevier Science. (Bottom right) Schematic representation of the edge and basal planes of highly ordered pyrolytic graphite (HOPG).

formed at graphite basal and edge planes (Figure 5).[115,116,119] The basal plane is the surface parallel to the graphene planes whereas the perpendicular surface is called the edge plane.[117] At basal planes, the SEI formed must be electronically insulating and impermeable to other electrolyte components, yet ionic conductivity is not requisite. Lithium cannot intercalate into graphene layers across basal planes thus SEI formation at these sites should be reduced to avoid loss of lithium inventory. The differing characteristics of the layers generated at basal and edge planes mean that true SEI formation potentials cannot be obtained by traditional electrochemical measurements.

The compositions of the SEI formed on the basal and edge planes of highly oriented pyrolytic graphite (HOPG) (Figure 5) are also different.[116,118] The basal plane manifests atomic flatness and low defect density while the edge plane contains dangling bonds, defects, sp^3 sites as well as functional groups due to the sudden termination of the lattice.[117] Thus, with more reactive sites on the edge planes, a denser and more homogeneous SEI layer is most often formed[119,120] and predominantly comprised of inorganic species of carbonates and semicarbonates[117] due to salt reduction, while on the basal plane, the SEI is comprised mostly of organic species of oligomers[117] due to solvent reduction. This was further confirmed by Argon sputtering of the SEI depth profile.[117] On edge planes, the SEI thickness does not vary considerably after the first cycle, as determined by in situ atomic force microscopy (AFM) measurements.[119,121] This suggests the SEI generated on the edge in the initial cycle is already both electronically insulating and ionically conducting.

For an electrolyte comprised of 1 M $LiPF_6$ in EC:DMC and highly ordered graphite, the SEI on the edge plane is believed to be several nanometers thicker than on the basal plane, in line with the observation of higher reaction current at the edge plane.[122–124] Nevertheless, the depicted SEI structure is influenced by the analyzing conditions, as even when the same electrodes and electrolytes were used the compositions varied. While the underlying cause of the differences between SEIs formed on HOPG basal and edge surfaces requires further examination in order to provide a fundamental and rigorous understanding of SEI formation, due to various hypotheses having been put forth to elucidate the molecular interactions at play between solvated complexes and graphite. An early study by Besenhard et al. suggests solvated lithium complexes intercalate between graphene layers which then decompose to form the SEI at the edge.[125] This was supported by Shkrob et al.'s finding that the EC derived SEI layer is polymeric, passivating the electrode surface.[126] Nevertheless, contradictions arise when PC is used as a network of linear polymers that does not hinder additional electrolyte decomposition.[126,127]

Another hypothesis is that lithium ions desolvate, thus they intercalate in between graphite layers at edge sites with remaining salt anions (which were previously bound to Li) decomposing to form inorganic species such as LiF.[115,128–131] In contrast, the basal planes are exposed to fewer (free) salt anions, but more unbound solvent molecules, hence a larger number of organic compounds are produced. However, the fast charge transfer kinetics on the edge plane can promote electrolyte

decomposition via electron transfer ring opening reactions of cyclic carbonates, producing radicals.[128,129] Such reactions may explain the larger proportion of alkoxides and carbonates identified on the edge plane than on the basal plane.[36,115]

In terms of properties, the model (ideal) SEI layer should be chemically stable against lithium, electronically insulating, ionically conductive and it must prevent lithium-electrolyte contact. Electron tunneling proceeds when the SEI thickness is <1 nm.[25] Although the electron tunneling during the initial SEI formation cycles is more pronounced as the primitive SEI layer is thin, once the thickness increases beyond this ≈1 nm threshold, electron transfer via electron tunneling is minimal. The ionic conductivity of the SEI is correlated with the species present in the multiphase layer, though the nanometer thickness and complex morphology render the determination of the ionic conductivity and Li^+ transport mechanism difficult using experimental techniques. Hence, theoretical methods along with indirect experimental observations were adopted focusing on the SEI structure and its individual components such as LiF and lithium alkyl carbonates.[132–137]

3.3. SEI Formation Mechanism: Reduction and Decomposition

Under extreme battery operating conditions, such as high temperature (>60 °C), high charge rate, and extended electrochemical cycles, results in either the growth of the SEI thickness or the loss of its protective ability, leading to performance deterioration via numerous aging mechanisms.[46,121,138] With the omission of PC, carbonate solvents utilized with the conventional electrolyte salt of $LiPF_6$ form stable robust passivating layers.[139,140] Though PC does perform well at low temperatures (<–10 °C) when used in conjunction with additives.[141] Further, the SEI layer formed on carbon-based anodes, such as graphite, has favorable microstructuring and properties with respect to other anode materials.[142–145] Several reduction processes compete on the carbon/graphite surface during charging. Typically, the reactants are solvents, salts, additives, and trace air impurities (e.g., water). The electrochemical reaction rates vary depending on their inherent properties, such as exchange current density, reduction activation energy, reductive potential as well as the identity of the reaction sites, basal or edge.[122,146,147] Hence, analyses of the SEI formation mechanism remain a core challenge due to the varying battery conditions and differing electrolytes employed.

Generally, carbonates from the electrolyte solvent precipitate with lithium ions to form Li_2CO_3, lithium alkyl carbonates, or other organic compounds while the salt ($LiPF_6$) forms LiF after reduction.[41] The standard reaction scheme for the reduction of cyclic carbonates is presented in **Figure 6**. Most reduction processes occur in the range of 0.8 V and 0.2 V versus Li/Li^+ on highly ordered graphite. The SEI formation process comprises of two steps, though the exact mechanism remains assiduously disputed.[41] In the first step, the graphite electrode is polarized, with the species in the organic electrolyte undergoing reductive decomposition generating new compounds. In the second step, the new compounds precipitate to form the SEI till all the graphite surface sites are covered. Most studies focus on the reduction pathways of solvent molecules particularly of carbonate-based solvents with $LiPF_6$ as these are the conventional electrolytes used in LIBs.

The reactions are driven by various factors, such as the lithium ion radius and the solvating power of the specific solvent used in the electrolyte which is related to its dielectric constant.[93,148] Lithium ions tend to be strongly solvated by solvent molecules, with solvents preferentially coordinating to lithium outcompeting anions. The concentration polarization causes solvated lithium ions to diffuse toward the graphite surface (edge sites) which then transform into the site for reductive decomposition reactions.[98] This is a critical step where competitive solvation of lithium by anion or solvent molecules dictates whether an electrolyte is destined to form a stable protective interphase. Yan et al. proposed several reaction pathways including 1) intercalation of desolvated lithium ions into the graphene layers, 2) heterogeneous transfer of electrons from the graphite electrode to the solvent molecules, 3) co-intercalation of the solvent molecules and the solvated lithium ions into the graphene layers and 4) heterogeneous transfer of electrons from the graphite electrode to the salt anions.[149]

The most spontaneous reaction is when desolvated lithium ions intercalate into the graphene layers at a potential more negative than the other competing reactions during cathodic polarization. Electron transfer from the graphite electrode to the solvent molecules as well as co-intercalation of solvated lithium ions into the graphene layers are the most debated pathways in the battery literature. The reduction of carbonate solvents follows either a one-electron or two-electron reduction process. In the one-electron reduction process a carbonate solvent, for example, ethyl methyl carbonate (EMC), produces an anionic intermediate species [$CH_3CH_2O(C^{\bullet}\text{-}O^-)OCH_3$] which subsequently reacts with Li^+ to produce CH_3CH_2OLi; whereas in the two-electron reduction process, for example, DMC, the reduction process involves the transfer of two-electrons and Li^+ to produce lithium carbonate and a gas.[150,151] In the case of EC, due to its high dielectric constant and high polarity, it is reduced in a one-electron transfer process at the graphite surface[79,126,127] to form an intermediate radical anion that then undergoes additional decomposition to form LEDC; a reactive species which reacts with trace water in the electrolyte to produce Li_2CO_3.[104,110]

However, it is proposed that EC actually undergoes a two-electron transfer reaction with Li^+ to form Li_2CO_3 and C_2H_4 (Figure 6).[72,125,152–157] The solvated lithium ions co-intercalate into the graphene layers forming intermediate graphite intercalated compounds (GICs) which are then reduced to form the SEI. Alternative reaction pathways involve the PF_6^- anion's attack on the EC molecule forming $CH_2FCH_2OCOOPF_3O^-$ and PF_5.[158–160] The $LiPF_6$ salt is thermodynamically unstable thus readily reacts with Li_2CO_3 to produce LiF, POF_3 and CO_2. The trace impurities such as H_2O and CO_2 in solution react with Li^+ to form Li_2CO_3, LiOH, and Li_2O, which form part of the SEI.[161–163] These species can accumulate on the electrode surface and may crack due to differing coefficients of thermal expansion of the deposit layer and the graphite.[164] Also, $LiPF_6$ reacts with water contaminations in the battery electrolyte releasing HF and HPO_2F_2 which are harmful species in case of leakage; whilst also detrimentally decreasing battery performance.[160,165] Hence, why it is imperative to keep impurity level in the electrolyte to a minimum.

The initial SEI components formed from conventional electrolytes are determined by the reduction products of EC and $LiPF_6$. The formation and growth of the SEI cause continual

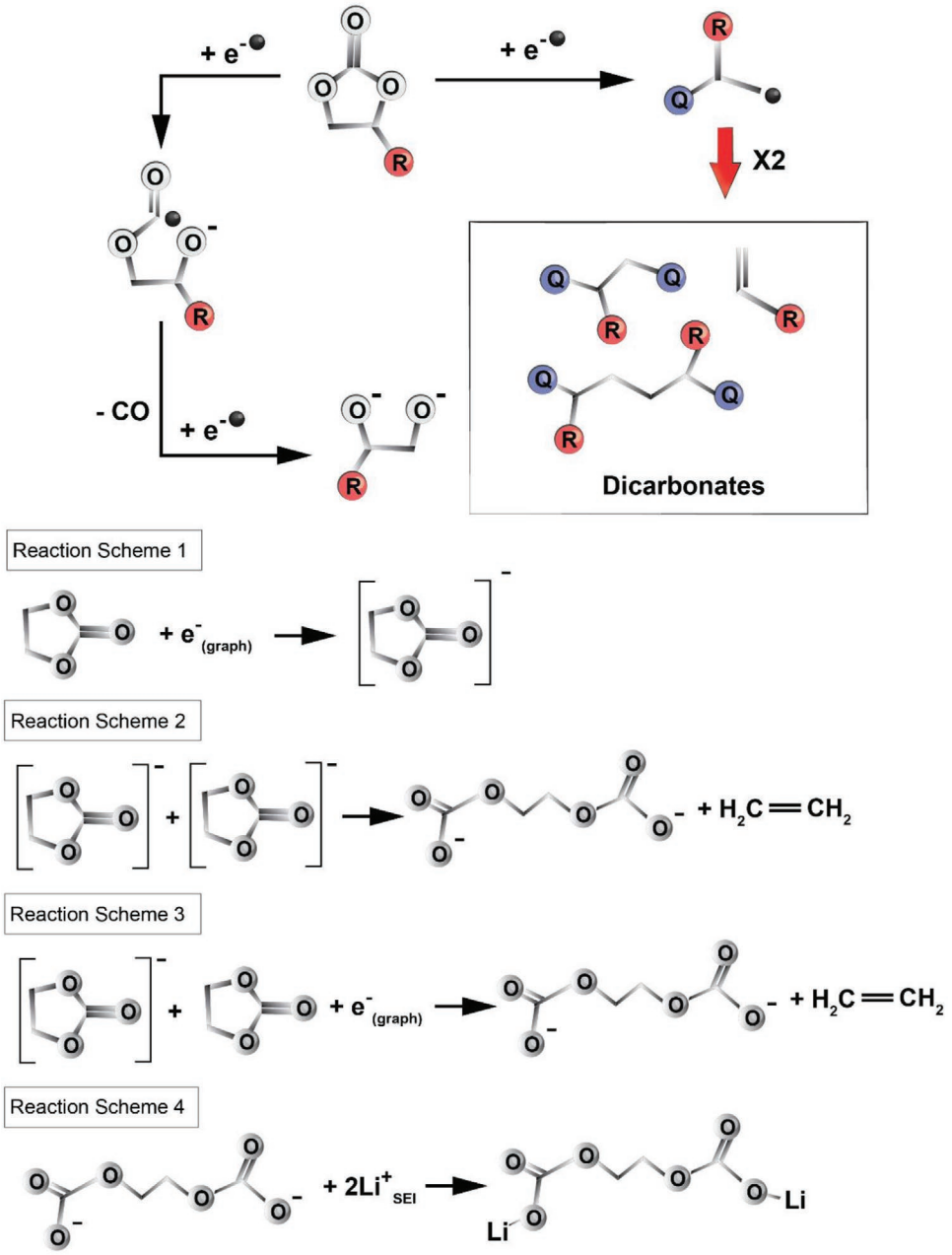

Figure 6. (Top) Putative reaction scheme for the reduction of cyclic carbonates and the formation of SEI components. Q represents the $-OCO_3^-Li^+$ group. Inspired by Shkrob et al.[126] (Bottom) The EC decomposition and precipitation pathway including the radical anion formation believed to be the rate-determining step (reaction scheme 1), formation of the ethylene dicarbonate anion (reaction schemes 2 and 3), and the precipitation of solid LEDC (reaction scheme 4).

changes in its composition, specifically an increase in the concentration of inorganic species, such as LiF and Li_2CO_3, and a decline in the concentration of organic compounds (lithium alkyl carbonates).[48] The initial SEI compounds are also unstable at the graphite anode and decompose to produce a mixture of species with mixed solubility in the electrolyte and gaseous species. Due to the decrease of insoluble compounds the SEI becomes progressively more porous over time. In LIBs using standard carbonate-based electrolytes the soluble species include ethers, fluorophosphates, and oligoethylene oxides. The insoluble species include LiF, Li_2CO_3, Li_2O, lithium carboxylates, lithium alkoxides, and lithium fluorophosphates, while the typical gaseous species are CO_2 and ethylene.[48] The presence of acidic impurities, for example, HF and PF_5, or transition metals, may catalyze these thermal decompositions, which are proposed to be the culprit for the disparate SEI compositions reported by different research groups. The varying conditions the cells are cycled in, as well as the higher ratio of electrolyte to electrode material utilized in experimental cells relative to commercial cells may result in an elevated

proportion of impurities accelerating the decomposition of the initial SEI components.[48,162,166]

A mechanism for the evolution of the SEI during aging was proposed by Heiskanen et al. (**Figure 7**) detailing the progression of the SEI composition following decomposition reactions.[48] In addition, the primary decomposition reactions of the SEI components are reported as follows: LEDC, a major component of the initial SEI (other than LiF), is unstable thus decomposes into a complex mixture of products (Figure 7).[167] With the SEI becoming progressively more porous, the electrolyte can access the surface of the graphite electrode facilitating additional reduction of the electrolyte to produce LEDC and LiF, forming the outer SEI layer. And with continued cycling further EC reduction and decomposition reactions take place leading to thickening of the layer, as well as more stable inorganic species concentrating near the surface. Consequently, the inner SEI consists primarily of inorganic species and the outer SEI is mainly comprised of solvent reduction products. Overall, the heterogeneous polydispersity of the SEI stems from the decomposition reactions of the initial products.

In addition to the growth-decomposition mechanisms in conventional electrolytes, more modernized electrolyte mediums have been formulated by tuning the solvation structure of the electrolyte; this is achieved by increasing the amount of lithium salt to achieve near-saturation concentrations. These systems differ in that Li^+ ions coordinate not only to solvents (as in conventional electrolytes), but they are also bound to anions. Consequently, the Li^+-anion-(solvating solvents)$_n$ ion sheath can participate in the SEI formation process. Such electrolytes are categorized as high concentration electrolytes (HCEs) and localized high concentration electrolytes (LHCEs).[168,169] As a result, the SEIs formed using these modern electrolytes predominantly consist of anion-based decomposition products, with the resultant SEIs formed deemed to be ionically more conductive.[170]

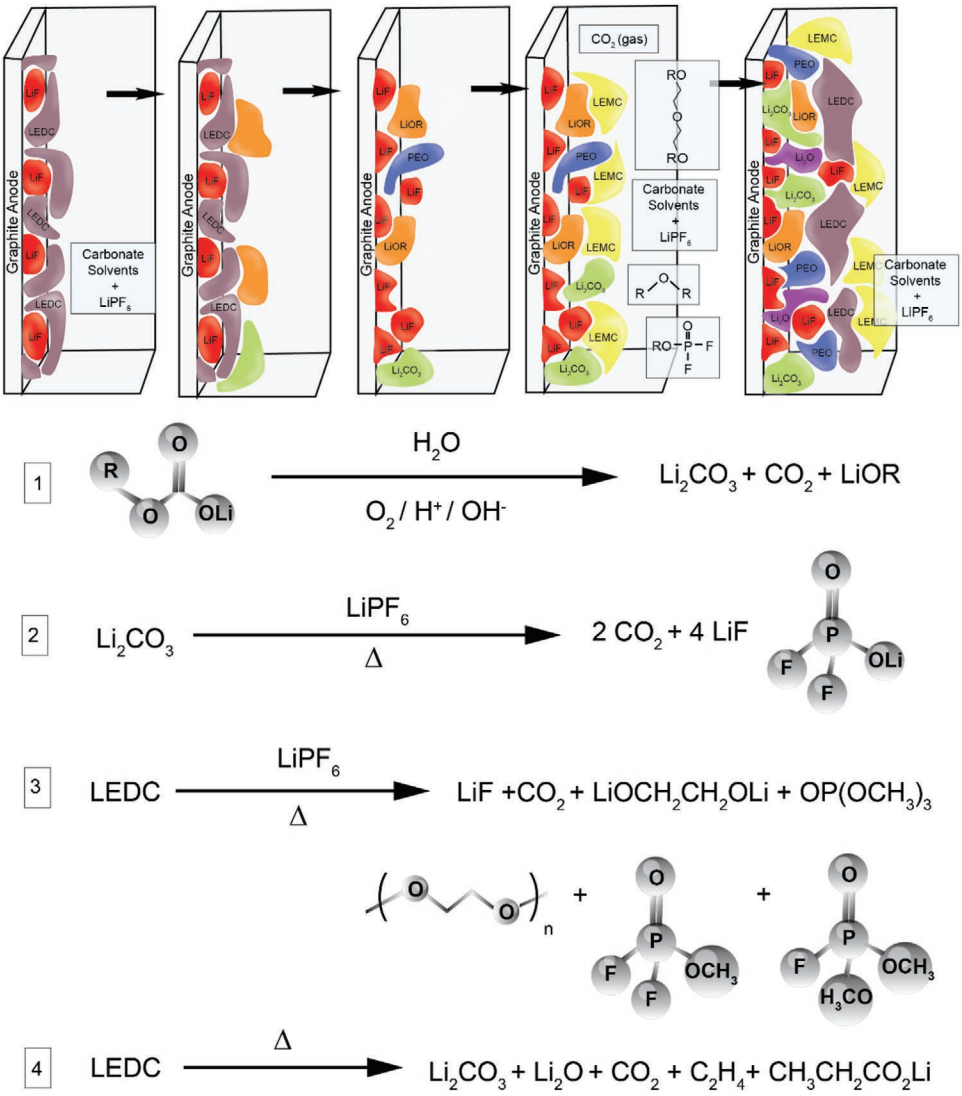

Figure 7. (Top) Initial SEI evolution on graphite showcasing the structure, thickening, and subsequent decomposition. Due to recent advancements in the characterization of the SEI components, lithium ethylene mono-carbonate (LEMC) has been included in this SEI representation.[171] This figure is inspired by Heiskanen and co-workers.[48] (Bottom) Primary decomposition reactions of the SEI species LEDC and Li_2CO_3.

3.4. SEI Evolution on Lithium Metal Anode

Works have shown that the SEI governs the practical application of LMBs, wherein: the SEI is responsible for transporting lithium ions as well as protecting metallic lithium from parasitic reactions with electrolytes.[24,25,32,45,172,173] Conversely, lithium plating/stripping is dictated by the composition, morphology, and thickness of the SEI which are related to the cycling stability of LMBs. However, due to the difficulty in the in situ and operando study of the electrochemical reactions occurring in an enclosed battery, including LMB, the exact features of the SEI remain unresolved. Owing to the high reactivity of lithium metal, it reacts with electrolytes forming the native SEI layer, which is usually fragile, non-uniform, and unstable, together with the driving force of the order-disorder transition ongoing in the SEI phase. In this case, the initially ordered system (electrodes, homogeneous electrolyte, etc.) evolves to a disordered phase with the formation of the SEI, itself highly disordered from nano-through to mesoscopic scales. The SEI itself has a gradient structuring from the anode and outward into the electrolyte bulk, one that is functional and requisite for high efficacy. Such disordering contributes to the rise of side-reactions and the formation of disordered lithium dendritic structures.[174,175] This native layer is easily eroded by the stress caused by electrode volume change and uneven lithium plating/stripping resulting in direct contact of lithium metal with the electrolyte. Subsequently, a new SEI layer is continually generated which causes continuous consumption of the electrolyte and lithium metal. What's more, the SEI can alter the distribution of lithium ions from the bulk electrolyte to the anode.[24] This occurs whereby the lithium ion is desolvated, diffusing through the bulk SEI with access to the Schottky vacancies pervading the layer. Eventually, the ion reaches the anode surface where it accepts an electron from the current collector before its deposition as Li metal.

In synthetic and laboratory settings, commercial lithium metal foil is usually utilized as the lithium metal. Due to the high surface reactivity with O_2, N_2, and H_2O when exposed to ambient air,[176] lithium metal foil is always covered by a layer of thin film comprising Li_2O, Li_2CO_3, and LiOH, which is naturally retained when used in LMBs. Though this layer on the lithium metal surface is stable, when put into contact with the electrolyte solution it spontaneously reacts with the solvent and anions within milliseconds or microseconds; postulated to even be as quickly as femtoseconds.[47] In LMBs an external voltage is applied to create an electric field between the cathode and the anode in order to activate the electrochemical plating and stripping of lithium ions. Subsequently, this results in the breakdown of the passivation layer on the lithium metal anode triggering additional reaction of exposed lithium metal with the electrolyte solution. With the use of lithium metal as the anode in LMBs, more lithium metal atoms are accessible for electrochemical reactions with the electrolyte solution therefore a greater supply of lithium leads to the formation of a "fresh" SEI during each cycle. The surface film formation on lithium metal anodes was examined by Aurbach et al. (**Figure 8**) in alkyl carbonates and 1-3-dioxolane solutions; supported by the associated and widely accepted schematic illustration of the process.[161,177]

On lithium metal anodes, the general SEI layer structure and composition as well as the electrolyte stability are similar to graphitic anodes, due to their similar reduction potentials, however, the electrochemical and thermodynamic stability of the SEI components differ.[178] If the initial SEI layer on a lithium anode is rich in inorganic species, it will prevent further Li metal-electrolyte reactions, thus slowing down the SEI growth.[173] The inverse occurs when the SEI layer is abundant in organic species, whereby a faster SEI growth rate is observed. Jiao et al. reported that the composition of the SEI layers in the same electrolyte varied with the Li capacity utilization and charge/discharge conditions.[179] The SEI layer on the lithium metal anode surface can be described as having three components. Firstly, the initial inorganic compounds formed before the anode are exposed to the organic electrolyte. Secondly, the insoluble inorganic and organic species are produced via chemical reactions between Li metal and organic electrolytes when the anode is saturated in organic electrolyte. Thirdly, the insoluble and partially soluble compounds are generated via the electrochemical reduction reactions of the electrolyte components. The SEI features on lithium metal anodes are contingent on the cycling conditions and electrolyte composition.

Dendrite formation is the main hindrance to the practical application of LMBs. Non-uniform lithium deposition promotes uncontrollable needle-like dendritic electroplating causing poor cycling efficiency and safety risks.[25,173] Heterogeneous lithium plating side reactions can occur caused by Li deposition/dissolution, though the inverse reaction, known as "stripping", can recover lithium metal. Uneven deposition and stripping of lithium results in the formation and growth of cavities, with reports showing that these regions stem from unevenly formed areas of the SEI; these cavities are electrochemically more active than flat surfaces, due to increased surface area: volume (SA: V) values.[180–182] Plated metallic lithium undergoes rapid reactions with the electrolyte to form the SEI, which can then electrically isolate the remaining Li to form "dead lithium," which cannot be recovered. Dead lithium manifests reduced conductivity and loss of lithium inventory with dendrites that can puncture the separator causing an internal short circuit. The Li morphology displays that dendrites possess a diameter of a few hundred nanometers, with dendrite growth shown to be dependent on the current distribution.[29,183,184] A key strategy to minimize the degradation of the lithium metal anode relies upon a uniform distribution of current density across the entire anode surface to promote dendrite-free deposition of lithium.

4. State-of-the-Art Approaches

Knowledge about the passivated interface between electrodes and electrolyte is crucial as this interface affects the capacity, cycling stability, properties, and safety of electrochemical energy storage devices. Nonetheless, there still lacks a comprehensive understanding encompassing morphology, phase, and chemical composition, especially on the nanoscale. The characterization of the SEI is difficult because it is a very thin layer with barely distinguishable boundaries with the electrolyte.[37,40] As a result, experimental analyses are challenging as it is difficult to ascertain the thickness of the layer on the carbon surface, making precise peeling off near impossible. As the chemical species of the solvent and SEI are similar, it is hard to discern which component belongs to the SEI and which to the electrolyte. This

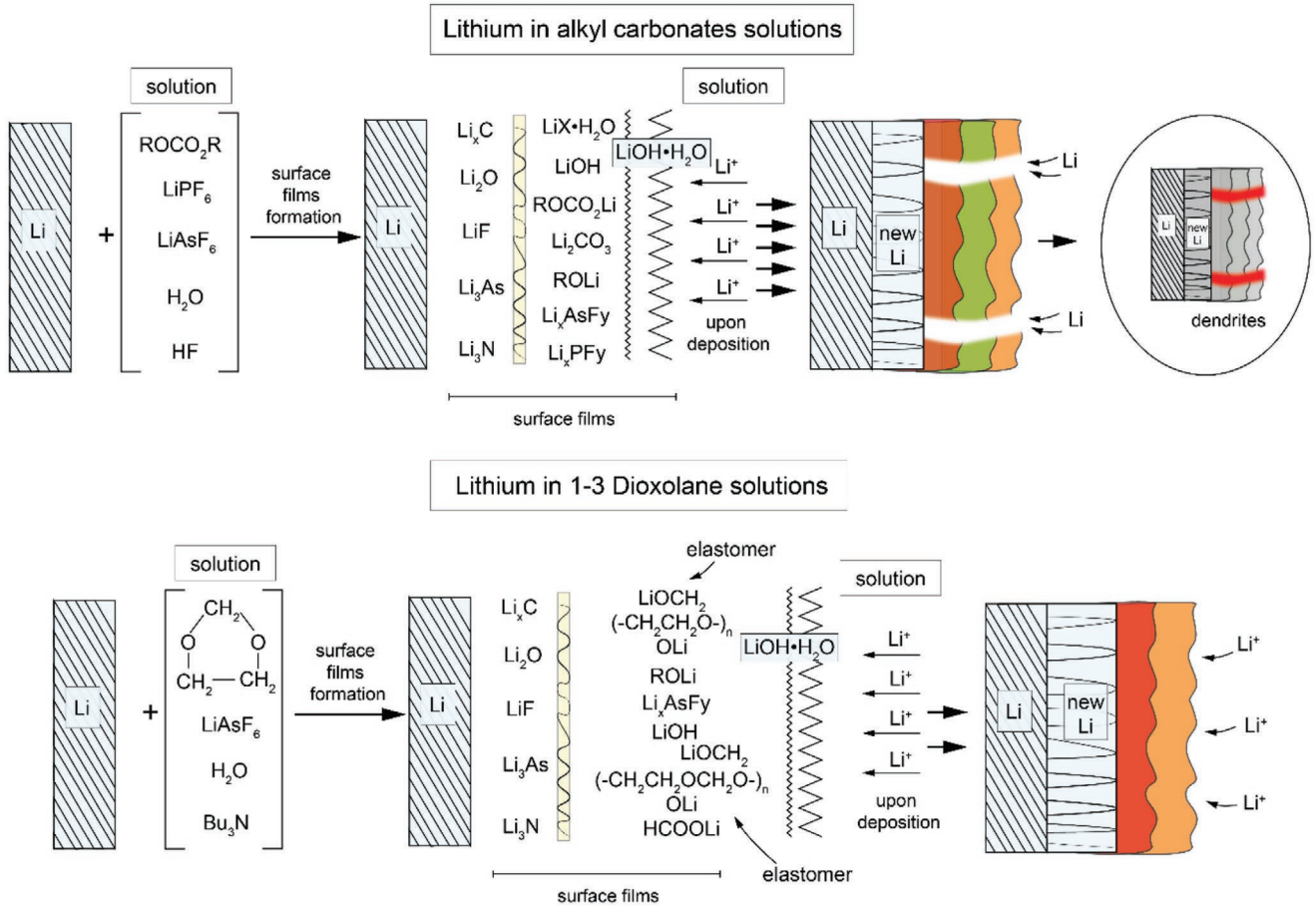

Figure 8. Schematic illustration of the surface film formation on lithium electrodes in alkyl carbonates and in 1-3 dioxolane solutions. This figure is inspired by Aurbach.[177]

is complicated by the sample preparation (separation, washing, and isolation) thus it is unlikely that the SEI maintains its original composition, with its components likely to undergo modification as well as degradation. Further, the components of the SEI are highly sensitive to air contamination and humidity, for example, ROLi and $ROCO_2Li$ can react with ambient CO_2 to form Li_2CO_3. It is also worth mentioning that SEI formation is affected by other factors including additives, concentration, current rate, state of charge, temperature, and voltage.

To characterize the SEI, specific experimental techniques ranging from microscopy to spectroscopy have been applied. To examine the surface of the layer, surface analysis techniques including AFM, scanning tunneling microscopy (STM), secondary ion mass spectroscopy (SIMS), and X-ray photoelectron spectroscopy (XPS) are used.[35,50,86,119,121,150,185–191] Whereas for imaging the surface film, SEM and transmission electron microscopy (TEM) are the preferred techniques, albeit retrospective to their destructive natures.[49,102,192–196] In addition, vibrational spectroscopies are employed to correlate surface information with functionality, including Fourier transform infrared (FTIR) and Raman spectroscopies.[76,164,197–203] The most commonly employed diffraction techniques include X-ray diffraction (XRD) and techniques that provide bulk information of the SEI components such as nuclear magnetic resonance (NMR).[77,109,171,186,204–208]

With the limitations of current experimental techniques to describe the SEI beyond its chemical composition, computational modeling has emerged as a feasible approach to making the structure of SEIs intelligible on length scales spanning the atomic and nanoscopic through mesoscopic, to the full battery systems.[99,209–214] The proposed mechanisms, such as the initial formation of the SEI layer through the reduction of the electrolyte on the anode surface via one- or two-electron reductions, needs to be verified with advanced techniques that can depict the reactions at the electrode/electrolyte interface at extremely small timescales (e.g., pico- or even femtoseconds). To explicate which electrolyte species are most susceptible to reduction, QC and molecular dynamics (MD) simulations have been employed, with a range of studies completed to calculate the redox potential of electrolyte species, in particular organic (carbonate) solvents and the conventional salt $LiPF_6$.[68,96,153,215–220] Other works characterized the decomposition mechanisms and reaction pathways of organic solvents (**Figure 9**), with particular foci on one of the most important components, EC.[155,221–223] Also, the oxidative decomposition pathways of carbonates and solvents were studied using QC calculations.[144,156,218,224] Note that such reduction mechanisms are involved in the initial SEI formation process, nonetheless, as these products accumulate on the electrode surface, they

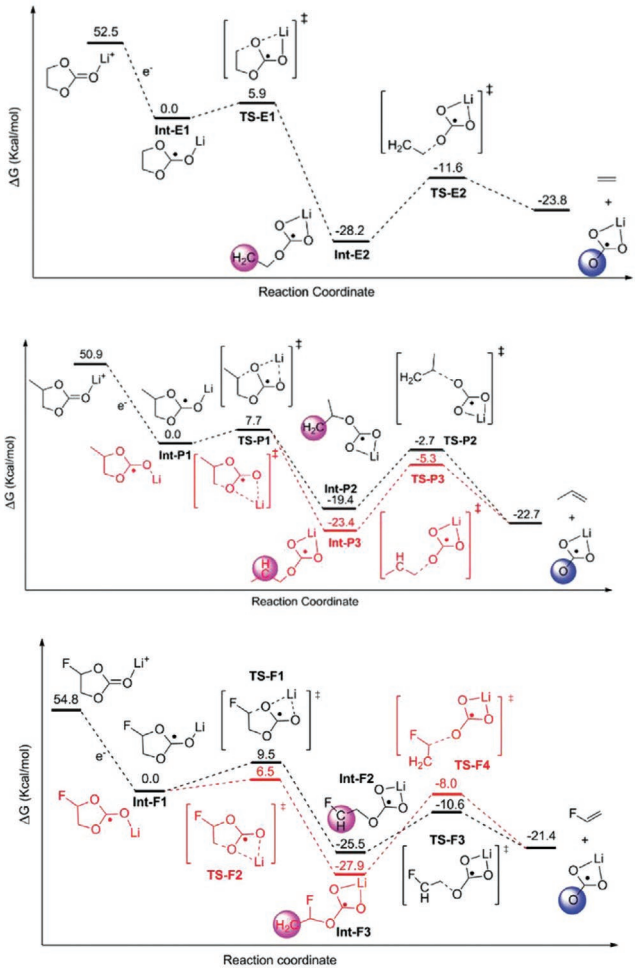

Figure 9. An exemplary computational study on the redox decomposition pathways of electrolytes. The calculated profile of free energy (ΔG) of EC (top), PC (middle), and FEC (bottom) decomposition assisted by lithium ions (the hydration energy of the solvated electron in water was −1.63 eV; the shaded areas denote the radical carbon and oxygen). Reproduced with permission.[156] Copyright 2021, The Royal Society of Chemistry.

undergo additional reactions as the surface becomes increasingly electronically insulating.

Toward the study of larger ensembles, ab initio MD (AIMD) has been performed to study the initial SEI formation process including the decomposition of EC on graphite surfaces.[222,225–227] AIMD has the advantage of computing the exact nuclear forces from the electronic structure without the use of a fixed chemical topology nor the approximations that typify classical force field based methods. This is aided by the use of periodic boundary conditions which provides the benefit of solvation effects in the bulk electrolyte or surface effects stemming from the electrode that can be fully captured, despite the limitation of unrealistic periodicity.[94,225,227–229] To enable simulations of larger system size and extended timescales, classical force fields such as condensed-phase optimized molecular potentials for atomistic simulation studies and the atomistic polarizable potential for liquids, electrolytes and polymers were developed.[230,231] Such classical force fields capture solution structures and transport properties of electrolyte, for example, 1 M $LiPF_6$ in EC or DMC as well as specific properties including cohesive energy, density, and solubility in the solvent.[230–233]

However, these force fields failed to describe the dynamic breaking of covalent bonds. The ReaxFF reactive force field was subsequently developed for Li—C—H—O systems that use a bond-order term along with a variable charge based on the electronegativity-equalization method (EEM) to describe covalent/ionic bond formation/breaking.[223,234,235] In the ReaxFF model, the electrons are treated implicitly prohibiting true simulation of redox processes (e.g., reduction reactions of EC) thus the eReaxFF method was developed which treats electrons explicitly circumventing this limitation.[236,237] Nonetheless, the parameterization of the reactive force field models necessitates continual advancements to accurately describe such complex systems.[238]

Recently, advancements in the study of the battery interphase were achieved using state-of-the-art computational and experimental approaches. To elucidate the nanoscale heterogeneity of the SEI, Raman signal enhancement techniques have been employed which use the plasmon resonance properties of metal nanostructures.[239] Such methods can deduce the composition of surface films on different electrode materials upon direct contact with organic (i.e., carbonate) electrolytes. This is exemplified by surface-enhanced Raman spectroscopy and tip-enhanced Raman spectroscopy (TERS), the latter utilized to study the amorphous silicon thin film anodes toward understanding SEI topography and chemical mapping.[201] TERS showed good correlation between the SEI structure and the distribution of LEDC and poly (ethylene oxide) (PEO) type-oligomer species. This technique is also applicable to the interphase in alternative battery chemistry such as Na-ion and multivalent redox systems. Furthermore, shell-isolated nanoparticle-enhanced Raman spectroscopy was used for the operando study of interfacial composition changes on tin (Sn) anodes upon cycling in LIB electrolyte.[202]

A concerted approach combining electrochemical quartz crystal microbalance (EQCM) and AFM[240] was applied to quantitatively monitor the interphasial species as they evolve on the electrode surface at various potentials in situ. EQCM is a highly sensitive mass monitoring technique that permits the weighing of species depositing on or that are lost from the graphite anode as a function of the applied potential. AFM images display how HOPG interacts with the solvated lithium ions during charge and discharge processes. LiF and lithium alkyl carbonates were identified by weighing the graphite anode with an EQCM, although the exact alkyl carbonate which was predominantly formed could not be resolved. Differential electrochemical mass spectroscopy further proved the preferential reduction of cyclic carbonates (over acyclic carbonate species); the primary components detected in the SEI. Relevantly, the probability for the SEI to be re-oxidized is dependent on its age, with the SEI on well cycled electrodes more difficult to re-oxidize.

The use of microscopy and spectroscopic techniques have been instrumental in resolving the composition and the thickness of the SEI.[102,195,196] The surface reactions of electrolytes were investigated by Nie et al. using binder-free graphite anodes allowing assessment of the SEI.[49] A combination of TEM with energy dispersive XPS along with solution NMR and FT-IR spectroscopy enabled the direct analysis of the graphite SEI of LIBs to establish that for EC/$LiPF_6$ electrolytes, the graphite SEI has a thickness of

≈50 nm after the first full lithiation cycle.[49] The layer was comprised of predominantly LEDC and LiF whereas upon alteration of the electrolyte composition, using EMC/$LiPF_6$, the graphite SEI is nonuniform and thinner (≈10–20 nm), containing lithium ethyl carbonate (LEC), lithium methyl carbonate (LMC) and LiF.

Wang and co-workers' study provided new insights into the composition of the SEI in LIBs which contradicts the current consensus that LEDC is the primary organic component.[171] Structural and spectroscopic characterizations suggest LEMC is the major product with complex interconversions and equilibria at play. The authors hypothesize that LEDC does not exist in the typical LIB environment due to the following reasons: (1) past studies have linked the organic SEI components to the LEDC standard which was actually LEMC; (2) LEDC is highly reactive to protio-impurities which are abundant in all cell assemblies, from trace moisture in bulk electrolytes to the graphite anode surface.[171] Therefore, LEDC cannot endure in this environment and even if it is formed via the one-electron reduction reaction, it is most likely to be converted to LEMC and LMC through reactions with protons and DMC. In addition, it was determined that LEMC possesses relatively high Li^+ conductivity which benefits the function of the interphase. Although the exact formation mechanism of LEMC remains to be established, such insights offer a clearer explanation of interphases and their specific properties relating to LIB performance.

A dynamic explanation of SEI formation in LIBs using operando liquid SIMS in combination with MD simulations[241] established that prior to any interphase chemistry occurring, an EDL forms at the electrode/electrolyte interface due to the self-assembly of solvent molecules. The formation of the EDL is guided by Li^+ and the electrode surface potential with the structure of the EDL (which becomes anion depleted, because the anions are expelled from the inner-Helmholtz layer structure once the electrode is negatively charged) predicting the eventual interphase chemistry. Simulation snapshots along with line plots of the ion distribution close to the Cu electrode and 1.0 M LiFSI in DME electrolyte with increasing voltage showed increasing Li^+ enrichment (**Figure 10**). The liquid SIMS chemical profiles reveal a structured SEI with a dense inorganic (predominantly Li_2O) inner layer (thickness ≈15–20 nm) that is LiF depleted while the outer layer is rich in organic species.

The effect of the electrode surface on SEI evolution was explored by Zhu et al. focusing on the differences in interphase formation on HOPG and disordered graphite electrodes.[242] The preferential formation of the SEI at graphite with defects over the HOPG was confirmed, supported by DFT calculations where the adsorption energy barrier of EC bound to Li is lower on the disordered graphite surface. The presence of defects led to the formation of a thinner, denser, and more uniform SEI on the electrode surface with stronger passivating capability as well as good stability upon cycling.[242] It was also reported that the defected graphite surface induced an SEI rich in LiF which aids the passivating component in the layer. This opens new vistas for the application of graphite with the defects as it can be coated onto conventional graphite electrodes along with other high-capacity electrodes (Li, Si, and Sn).

First-principles simulations of the thermodynamic, kinetic, and electronic properties of the interface between LiF and Li_2CO_3 showed a significant reduction in the activation barrier for Li transport, due to the interface possessing the highest Li ion diffusion coefficient.[234] As we note, this study was conducted on a crystalline SEI structure and thus we highlight that

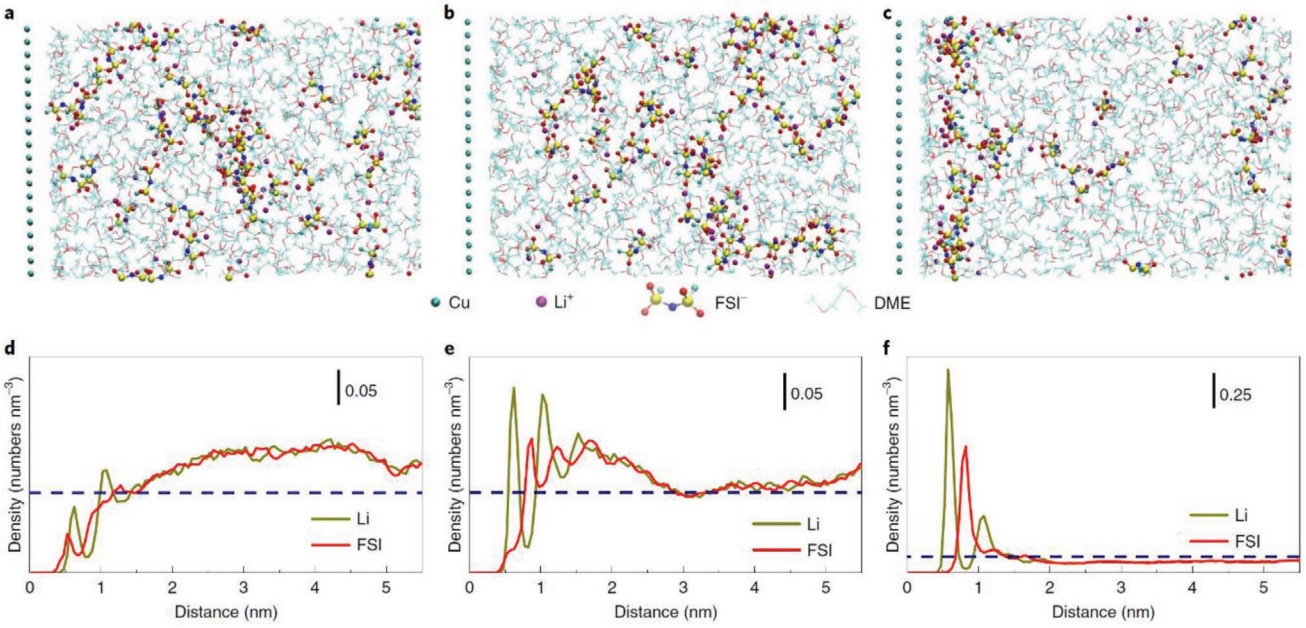

Figure 10. Simulation snapshots and line plots of the ion distribution near a Cu electrode and a 1.0 M lithium *bis*(fluorosulfonyl)imide (LiFSI) in 1,2-dimethoxyethane (DME) electrolyte interface with increasing voltage. Snapshots (top) from the simulation at a) 0 V, b) 1.0 V and c) 2.8 V with Cu electrode on the left and the ion distributions near the anode. The corresponding line plots of the ion distribution are shown in (d), (e), and (f). When no potential was applied no Li^+ enrichment at the interface was detected, as shown in (d). (e) and (f) suggest the thickness of the EDL is less than 1 nm. As a higher potential is applied the Li^+ enrichment at the electrode/electrolyte interface becomes more significant, comparing (e) and (f). (The dashed lines indicate an even distribution). Reproduced with permission.[241] Copyright 2020, Springer Nature.

one must consider the different compositions of the interfaces with the possibility of amorphous regions being generated in the multiphase SEI which will alter the Li-ion diffusion pathways, in-turn impacting the ionic conductivity of the phase. As the SEI is heterogeneous, this may manifest as a myriad of differing current densities across the electrode/electrolyte interface, hence a combination of computational and experimental approaches is required to understand the disordered interfacial behavior, toward informing on the design of next-generation batteries.

5. Standing Problems and Outlook

5.1. Standing Problems

The development of battery electrolytes has thus far been primarily led by empirical observations culminating in the discovery of EC as a viable electrolyte that can actively passivate graphite. The absence of a structure-property relationship between electrode and electrolyte materials hinders the rational optimization of LIBs, as well as next-generation battery chemistry. Current modeling efforts rely on the proposed SEI structures and mechanisms, as the continual evolution of the SEI represents a theoretical challenge due to changes in the interphase microstructure spanning different lengths and time scales. The computational approaches that have been employed thus far are performed only on idealized ordered and often periodic systems. Due to the multi-component polydispersive nature of the SEI, an encompassing model which captures the various phenomena and effects has yet to be established; one that includes heterogeneities and functional disorder.

Computational models of the SEI are limited by a compromise in accuracy between the inverse capability for ensemble size (number of atoms/particles) and energetic-temporal resolution. Weakly-polar interactions, dispersion forces, and accurate descriptions of vibrational dynamics being essential to accurate characterization of electrostatic behavior, yet computationally costly and thus limiting system size. Existing state-of-the-art atomic and continuum scale simulation methods cannot fully characterize the interphase thus simplification of the system description, governing (physics) equations, and parametric scale bridging must be applied.

The study of the SEI is also hampered by the lack of experimental techniques which afford the nanoscale or resolution for elucidating the SEI structure and the pico- or even femtosecond temporal resolution in relation to the electrode potential and electrochemical reactions. To avoid exposure to ambient conditions that can alter the integrity of the layer, non-destructive and in situ techniques must be effectuated. The widely used in situ microscopies (AFM, TEM) provide minimal molecular information, while XPS and XRD also lack the spatial resolution necessary to correlate the chemical insights with the electrochemical interface. XRD monitors the entire electrode thus it cannot distinguish specific interactions on the electrode surface between particles and electrolytes. Even the most advanced analytical techniques such as cryogenic TEM resolve SEI structural and chemical information, yet, it cannot provide details of the dynamic growth features in the layer under actual operating conditions.[243,244] While microscopic and spectroscopic techniques are restricted by typical operating temperatures/pressures far from the battery ambient range (the latter also by selection rules); the acquired results and conclusions are likely qualitative at best.[245]

The remaining issues for the characterization of the SEI stem from the conflicting reports on the exact composition and properties. This is exemplified by the controversy over the existence and role of LiF in the SEI with some studies stating it is not present in the dense inner SEI layer, nor does it have a protective function for limiting the electrolyte decomposition.[32,196,204,240,241,246] To avoid such contradictions necessitates a shift to in situ operando techniques to characterize the battery during operation. Batteries function in a closed environment and only when the device is opened can researchers analyze the state of the electrolyte and electrode materials, hence necessarily retrospective with the system possibly altered by change of conditions from operating ones. Collaborations across disciplines with collective advances in theoretical methods, experimental capability, and advanced characterization techniques can overcome these limitations in the study of battery interphases.[247,248]

Lastly, toward the development of high energy density batteries using modern electrolytes requires the use of different additives, typically up to 5% per volume or weight. The introduction of additives further increases the complexity of the reactions which occur at the electrode/electrolyte interphase. Additives such as vinylene carbonate (VC) or fluoroethylene carbonate (FEC) have been studied extensively and are reported to be preferentially reduced on the anode to produce an enhanced SEI, ameliorating the cycle life of LIBs. The use of electrolyte additives generates SEI components with improved stability that impede decomposition, evolution, and thickening of the SEI layer. However, the mechanisms of such additives, their functionality, or how the SEI is modified remains ambiguous. As a result, the understanding of the next generation lithium and post-lithium batteries requires comprehensive advancement to ascertain how electrolyte additives affect the SEI composition, morphology, and eventual properties.

5.2. Outlook

A key facet for the future design of the SEI layer lies in establishing the structure-property relationship of the interphase. Albeit challenging, the main properties that the SEI must possess have been defined. Firstly, the SEI must be ionically conductive yet electronically insulating, it must not impede Li-ion transport from the electrolyte to the electrode, the layer must be chemically stable not reacting or dissolving into the electrolyte and the SEI must be mechanically stable; it should not crack or undergo volume expansion during charge-discharge cycles. The large volume change is one of the primary concerns for alloy anode (e.g., Si, Sn, aluminum, magnesium) design and development, though progress has been made incorporating carbon additives or a carbon coating, as exemplified by silicon composite anodes.[55,249–251] However, the criteria outlined herein will not be met by a single component of the SEI due to the polydispersive nature of the layer, hence it is paramount that a structure-property relationship is developed in relation to the SEI species and one that accounts for dynamics and structure, as well as the ensuing disorder in the evolving SEI architecture. Another key factor is the appropriate thickness of the SEI for

optimal battery performance; reported to be in the range of a few up to ≈20 nm.[41,168,252]

The rational development of an artificial SEI offers a viable option toward the rational optimization and tailoring of the ideal chemistry and features of the multi-layer interphase. The artificial SEI can be advanced through predictive computational modeling, particularly when combined with knowledge and precise characterization of relevant electrode surface-coating technologies. Methods such as atomic layer deposition (ALD) and molecular layer deposition (MLD) can deposit a conformal thin insulating coatings of uniform distribution and thickness at the atomic scale on electrode surfaces.[253–258] Regardless, the rational engineering of a stable SEI will involve a transition to employing complementary techniques across three main areas: computational modeling, machine learning models, and advanced operando experiments.

5.2.1. Computational Modeling

To develop a framework for the comprehensive characterization of the SEI structure, order-disorder transitions, dynamics, and functional properties, it is essential to consider all the factors that influence its formation. Specifically, the electrolyte along with the solvation structure of lithium ions and the EDL behavior at the interface determines the preferential reduction reactions during SEI formation.[259] Computational methods that take into account the full electronic structure at the atomic scale are requisite to quantitatively characterize the SEI formation and evolution with descriptors and interpretation complementary to ML and operando experiments.[260] A reductionist approach can be employed in the construction of electrolyte complexes which can then be evolved to larger clusters, whilst retaining the specificity arising from differing 3D structures and oscillations between poses and forms. DFT calculations can compute the specific inter- and intramolecular interactions in electrolyte systems (including Van der Waals, dispersion, etc.) providing information on structural configurations, conformations, and dynamics as well as reaction mechanisms that underpin electrolyte behavior. These details can be incorporated into large scale models or used to better-parameterize these, toward providing an ever evolving meso- and macroscopic understanding of the SEI.

AIMD is suitable for the large scale simulation of electrolyte systems to acquire time-resolved information of the SEI formation and functional mechanisms. This permits the scale-up of base-descriptors from DFT calculations from atomistic to nanoscopic-mesoscopic insights and beyond. The ReaxFF and eReaxFF reactive force fields can also be utilized to simulate electrolyte solvent decomposition reactions as bond breaking/formation are sufficiently well described by empirical potentials to generate semi-quantitative information. Modeling of larger systems is essential to elucidate the dynamic interfacial structures and interactions as well as the long-range order structure, especially with increasing evidence of EDL impacting the resultant SEI formation.[259,261–263] First-principles methods for open quantum systems can be employed to investigate the electronic structures at the SEI-anode and SEI-electrolyte interfaces.[264] Time-dependent DFT open system method[264–267] can be used to simulate in real-time the electron injection, reduction reaction, and SEI formation.

Ultimately, continuum models are efficient computational methods to simulate the bulk electrochemical performance of batteries and are usually coupled with physical degradation models, for example, SEI formation and growth during the charge/discharge process. The main continuum models that can be employed include the following: single particle (SP) model, pseudo-2D (P2D) model, pseudo-3D (P3D) multiscale model, phase-field model, and 4D-resolved model.[213,268,269]

5.2.2. Machine Learning Models

ML is a type of artificial intelligence that can extract information from large datasets, with algorithms that build a model based on sample data, leveraging the data for predictive outcomes. ML potentials are a mathematical representation of the 3-N dimensional potential-energy surface, which is the total energy and interatomic forces for a given set of N atomic centers.[270] Such models "learn" the correlation between structure and energy/forces from data acquired through simulations. These models are only limited by the quantity and quality of the reference data used to train them, with the computational cost of ML-based force fields only dependent on the choice of the model but not the complexity of the interactions.

Three state-of-the-art ML models exist that can be combined with atomic and electronic simulations.[44] Neural network potentials use predetermined structure fingerprints of the local environment, these models can handle complex systems and large data sets. Gaussian process regression utilizes structural fingerprints such as Smooth Overlap of Atomic Positions (SOAP) which are data efficient. Graph neural networks learn the fingerprints and map them to the energy and forces. Such models are applicable to study the SEI using the automated learning of the most efficient fingerprints and the graph data structure which is related to the atomic structure. ML models have been incorporated with atomic and electronic simulation methods therefore the foundation is present to expand upon existing ML potentials extending their capabilities for complex systems.[271–278] To build effective ML potentials to model the SEI, they must consider electrostatic interactions and determine accurate structures in reaction pathways that deviate from equilibrium. In addition, to enhance the accuracy of the ML models, advancements in the description of inter/intramolecular forces and short/long-range interactions need to be implemented. Ab initio methods are computationally demanding approaches while force field methods can model larger systems yet compromise accuracy. ML models can bridge this gap for the study of progressively larger chemical systems such as the SEI, at ab initio accuracy with force field efficiency.[271] It is important to note that, despite their wide applications, ab initio methods are not as accurate as required; ML has been employed to improve the DFT's accuracy.[273,279,280] The ML-assisted ab initio methods can be used to ensure the reliability of the simulation results.

5.2.3. Advanced Operando Experiments

As batteries function in a closed environment and the SEI formation, composition and evolution are interfacial dynamical

processes, in situ and ultimately operando characterization techniques present unique advantages. Among the techniques under development, those that utilize non-destructive and non-ionizing probes with high material penetration depth, offering lithium battery-relevant energy/frequency range and spatio-temporal resolution have the most potential for breakthrough. In this sense, neutron and terahertz (THz) probes have intrinsic advantages over X-ray, electron, and optical techniques.

In situ neutron scattering at pulsed sources offers time-resolved information on a sample's atomic/nano- through meso-, to macro-scale structuring for crystalline, amorphous, liquid, and even gaseous components of systems under study. Further, quasi-elastic neutron scattering (QENS) techniques can provide information on ionic, atomic, and molecular diffusions and rotations, whilst inelastic neutron scattering (INS) measurements can resolve collective, cooperative whole system vibrations (i.e., phonon modes) through to higher-energy localized vibrational dynamics. Neutron Compton scattering (NCS), also termed "deep-INS" (DINS), albeit particularly rare, provides a unique opportunity to resolve and track element-specific kinetic energies, which are related to atomic cohesions and thus bonding strengths on the nano-scale, whilst also being relevant to bulk and physical properties;[281] thus able to provide a glimpse into the evolving properties of the SEI and in real-time, as with other disordered and amorphous systems. QENS, INS, and NCS operate via determination of energy change of the incident and subsequently scattered neutrons after they interact with atoms in the sample system, to determine the quantized momentum transfers to the sample (similar to absorption-specific energetics in optical techniques).[282] Being charge-free, neutrons are non-ionizing, non-destructive, and do not interact with electrons, instead directly interacting with the nuclei. Neutrons easily penetrate ≈1–2 cm of most materials and thus have the ability to probe the relationship between structure and electrochemical performance in battery materials under operation, as being employed in other energy and climate related systems (eg. CO2-mineralisation and carbonation). The high sensitivity of neutrons to Li[283] can precisely quantify Li content and its manifold density at the anode surface, including its adsorption or insertion into the porous framework[283] and subsequent Li-containing component deposition/decomposition in the SEI layer.[284–288]

Neutron reflectometry, in particular in situ neutron reflectometry (NR) offers advantages over ex situ techniques, such as XPS,[289] time-of-flight SIMS and FTIR. These ex situ techniques are necessarily retrospective due to technical and experimental limitations and thus are not resolving phenomena neither at an active electrode, nor one in contact with the electrolyte.[289] In NR measurements, neutrons are reflected from most materials at grazing angles and the absorption is neglected[290] so the total number of neutrons remains constant via the sum rule, from which SEI thickness, density, chemical nature, and structural evolution can be elucidated.[291–294]

With respect to the resonance frequencies of the electrons and vacancy-defects in a doped semiconductor, these appear in the low-energy or "THz regime" and together with the electronic conductivity also having a dynamic component in the THz frequency range, where THz time-domain spectroscopy (THz-TDS) can be employed. This low-energy far-IR range, also termed the fingerprint region, presents challenges for performing measurements due to the lack of compact, high-power, and low-consumption solid state coherent sources and efficient detectors. Opportunely, the rapid development of relevant technology for the generation and detection of coherent THz radiation has made this frequency region more accessible and with high-resolution. The general description of THz spectroscopy refers to techniques that employ coherent (heterodyne) transceivers as opposed to the incoherent (noise) sources, as historically used in far-IR spectroscopies. Furthermore, THz radiation suffers less from scattering compared to IR due to the larger wavelength, while remaining non-ionizing (non-destructive), while allowing it to penetrate deeper into materials whilst not contributing to changes in the sample, especially important for time-dependent measurements. THz-TDS most often operates in the ≈0.1–10 THz frequency range (10^{11} – 10^{13} Hz ≈ 0.41–41 meV) and provides contact-free, non-destructive characterization through measurable frequency-resolved attenuation of the reflected/transmitted THz field following its interaction with a sample.[295] The measured time-resolved THz signals can be converted to battery-related parameters depending on the experimental setup. For example, THz-TDS can help resolve aspects of the ionic conduction mechanism[247] as well as SEI formation and evolution[248] in response to external stimuli, such as the applied voltage or current and their time duration in LIBs.

As neutron and THz probes interact with all the atoms in the beam path of a bulk sample, the design and placement of the in situ multi-component electrochemical cells for interaction with the components of interest, as well as material selection, are all crucial for achieving high signal/background ratio and minimal multi-scattering. Traditional experimental techniques (e.g., impedance analyses) should be used in conjunction to assist data interpretation. Indeed, as with all empirical determinations the trends emerging from neutron and THz measurements become even more intelligible when a synergy is formed with related computational simulations of the phenomena being probed.

However, neutron and THz techniques are not without their own shortcomings and challenges, including first and foremost access, where both techniques are rare at best and neutron scattering only available at large-scale facilities. Further, the amount and size of sample required are relatively large in terms of size, volume, or weight often at the limit or beyond of prototype systems or materials employed in laboratory determinations; potentially limiting their study due to availability and/or cost. Even with sufficient sample, neutron scattering also presents challenges of analyses and interpretation due to the relative novelty of the techniques in the context of complex or applied systems, with a much smaller experiential literature to draw upon.

Further, the scattering cross section of each element widely differs with some presenting a significant challenge to resolve, especially in the presence of "good scattering" ones; H-atoms being the best scatterers, yet only in forward scattering due to the matching proton-neutron mass, back-scattering is not possible off of H-atoms. Organic solvents and systems containing C, O, N, S can also be transparent to neutrons, especially in the presence of high-H content samples due to their smaller coherent absorption cross sections (relative to H). ^{1}H also has a large incoherent cross section; hence in diffraction

experiments will contribute background, which if troublesome, can be eliminated by using deuterated solvents. Otherwise, this incoherence "clouding" measurements can be addressed by carrying out comparative measurements tracking changes over time, in differing environments (i.e., temperature, solvent) else diverse concentrations toward generating relative trends. Analyses can be limited to the back-scattering or on the differences between front and back-scatter, yet the loss-of data from eliminating front-scattering can significantly limit some measurements. The lack of structural or dynamic information can also be accessed with cryogenic TEM and ultra-high resolution SEM and TERS to probe and to help resolve the morphology, nanostructure, and nanoparticle grain boundaries in lithium-ion transport through the SEI.[296,297]

To summarize, a unified cross-discipline approach merging modeling, artificial intelligence, and large-scale facility experiments within a centralized framework will transition battery research toward innovative discoveries (**Figure 11**). Cultivating

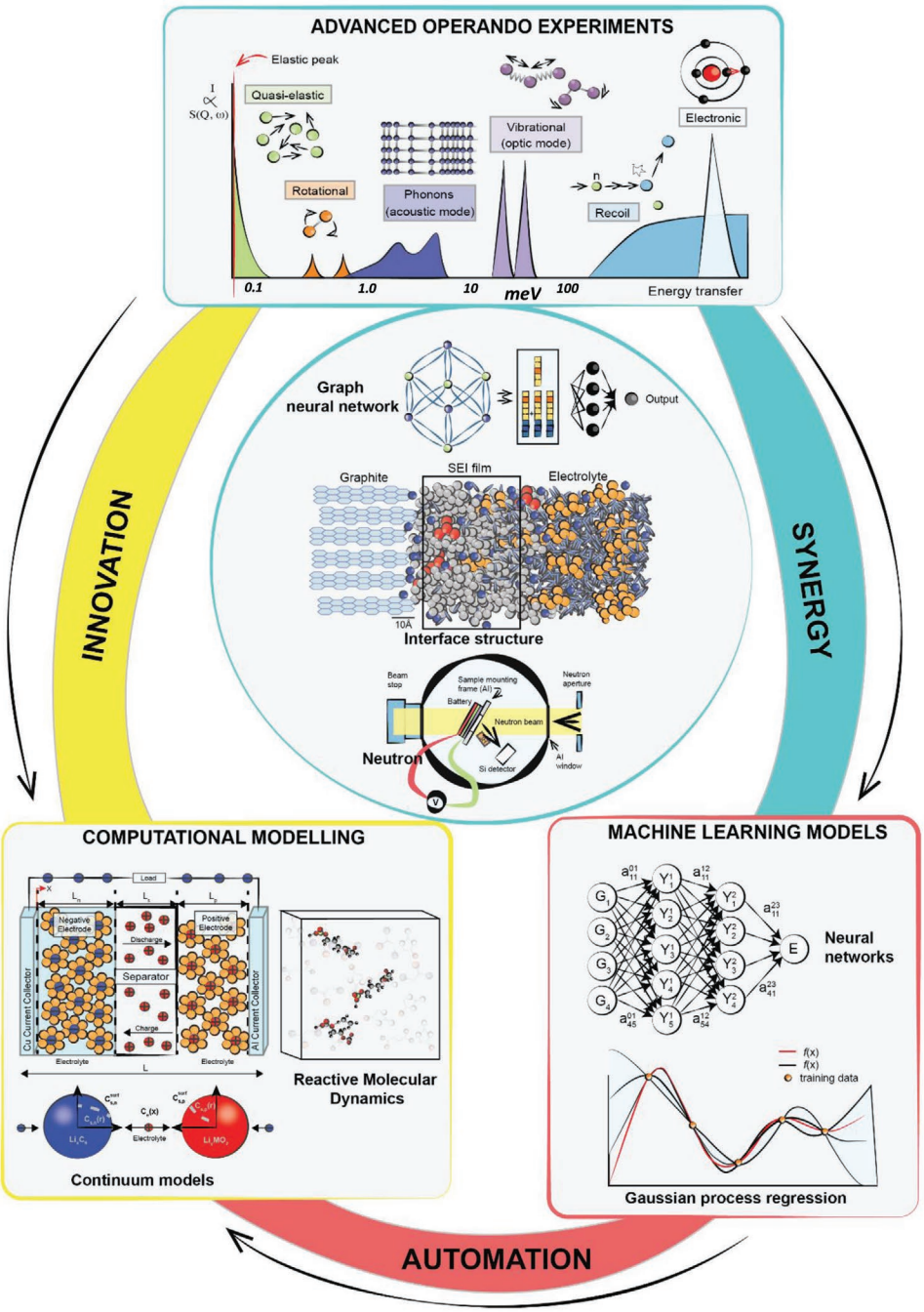

Figure 11. Summary outlook detailing the innovative cross-discipline characterization techniques which can provide a means to resolve the SEI complexities.

a synergistic approach will ensure an accurate characterization of the SEI to resolve its dynamic spatio-temporal features and develop superior battery technologies.

Acknowledgements

The authors would like to thank Miss Stephanie Ferreira for her graphical expertise in constructing Figures 1–4, 6–8, and 11. H.A. acknowledges the Hong Kong Quantum AI Lab Limited for supporting his fellowship. G.A.C. acknowledges the EU-Horizon 2020 and BEIS, UK for supporting the FUNMIN project (ACT, No. 299668), and the RAL-ISIS neutron and muon facility, STFC, UK is thanked for supporting the following funding related to the evolution of the neutron science covered in this work: RB1710285, RB1710444, RB1710447, RB2010426, RB2010696. S.P. acknowledges the basic funding from the Helmholtz Association. K.V.T. thanks Prof. Bruno Botta (Sapienza University of Rome), Prof. David H. Farrar and the Department of Chemistry and Chemical Biology (McMaster University), as well as Prof. Rickey Y. Yada and the Faculty of Land and Food Systems (University of British Columbia) and the Natural Sciences and Engineering Research Council, Canada (RGPIN 04598, RYY) for support. G.C. acknowledges the support from the Hong Kong Quantum AI Lab Limited, AIR@InnoHK of Hong Kong government.

Conflict of Interest

The authors declare no conflict of interest.

Keywords

Helmholtz double layer, lithium metal batteries, lithium-ion batteries, solid electrolyte interphases, Stern Helmholtz layer

Received: September 30, 2022
Revised: December 7, 2022
Published online: January 18, 2023

[1] S. Chu, Y. Cui, N. Liu, *Nat. Mater.* **2016**, *16*, 16.
[2] J. Amici, P. Asinari, E. Ayerbe, P. Barboux, P. Bayle-Guillemaud, R. J. Behm, M. Berecibar, E. Berg, A. Bhowmik, S. Bodoardo, I. E. Castelli, I. Cekic-Laskovic, R. Christensen, S. Clark, R. Diehm, R. Dominko, M. Fichtner, A. A. Franco, A. Grimaud, N. Guillet, M. Hahlin, S. Hartmann, V. Heiries, K. Hermansson, A. Heuer, S. Jana, L. Jabbour, J. Kallo, A. Latz, H. Lorrmann, et al., *Adv. Energy Mater.* **2022**, *12*, 2102785.
[3] M. Armand, J. Tarascon, *Nature* **2008**, *451*, 652.
[4] M. Winter, R. J. Brodd, *Chem. Rev.* **2004**, *104*, 4245.
[5] G. E. Blomgren, *J. Electrochem. Soc.* **2017**, *164*, A5019.
[6] R. Marom, S. F. Amalraj, N. Leifer, D. Jacob, D. Aurbach, *J. Mater. Chem.* **2011**, *21*, 9938.
[7] J. W. Choi, D. Aurbach, *Nat. Rev. Mater.* **2016**, *1*, 16013.
[8] J. B. Goodenough, Y. Kim, *Chem. Mater.* **2010**, *22*, 587.
[9] F. Duffner, L. Mauler, M. Wentker, J. Leker, M. Winter, *Int. J. Prod. Econ.* **2021**, *232*, 107982.
[10] K. Liu, Y. Liu, D. Lin, A. Pei, Y. Cui, *Sci. Adv.* **2018**, *4*, eaas9820.
[11] Y. Liu, R. Zhang, J. Wang, Y. Wang, *iScience* **2021**, *24*, 102332.
[12] M. Armand, J. M. Tarascon, *Nature* **2001**, *414*, 359.
[13] Y. Chen, Y. Kang, Y. Zhao, L. Wang, J. Liu, Y. Li, Z. Liang, X. He, X. Li, N. Tavajohi, B. Li, *J. Energy Chem.* **2021**, *59*, 83.
[14] H. Zhang, C. Li, G. G. Eshetu, S. Laruelle, S. Grugeon, K. Zaghib, C. Julien, A. Mauger, D. Guyomard, T. Rojo, N. Gisbert-Trejo, S. Passerini, X. Huang, Z. Zhou, P. Johansson, M. Forsyth, *Angew. Chem., Int. Ed.* **2020**, *59*, 534.
[15] J. Xie, Y. C. Lu, *Nat. Commun.* **2020**, *11*, 9.
[16] S. Flandrois, B. Simon, *Carbon* **1999**, *37*, 165.
[17] Y. S. Duh, K. H. Lin, C. S. Kao, *J. Therm. Anal. Calorim.* **2018**, *132*, 1677.
[18] S. Megahed, W. Ebner, *J. Power Sources* **1995**, *54*, 155.
[19] X. Zeng, M. Li, D. Abd El-Hady, W. Alshitari, A. S. Al-Bogami, J. Lu, K. Amine, *Adv. Energy Mater.* **2019**, *9*, 1900161.
[20] L. Lu, X. Han, J. Li, J. Hua, M. Ouyang, *J. Power Sources* **2013**, *226*, 272.
[21] J. Wen, Y. Yu, C. Chen, *Mater. Express* **2012**, *2*, 197.
[22] M. J. Lain, E. Kendrick, *J. Power Sources* **2021**, *493*, 229690.
[23] K. Xu, *Chem. Rev.* **2004**, *104*, 4303.
[24] X. B. Cheng, R. Zhang, C. Z. Zhao, F. Wei, J. G. Zhang, Q. Zhang, *Adv. Sci.* **2016**, *3*, 1500213.
[25] H. Wu, H. Jia, C. Wang, J. G. Zhang, W. Xu, *Adv. Energy Mater.* **2021**, *11*, 2003092.
[26] X. Liu, D. Ren, H. Hsu, X. Feng, G. L. Xu, M. Zhuang, H. Gao, L. Lu, X. Han, Z. Chu, J. Li, X. He, K. Amine, M. Ouyang, *Joule* **2018**, *2*, 2047.
[27] R. Padbury, X. Zhang, *J. Power Sources* **2011**, *196*, 4436.
[28] G. Di Donato, T. Ates, H. Adenusi, A. Varzi, M. A. Navarra, S. Passerini, *Batteries Supercaps* **2022**, *5*, 202200097.
[29] J. N. Chazalviel, *Phys. Rev. A* **1990**, *42*, 7355.
[30] X. B. Cheng, Q. Zhang, *J. Mater. Chem. A* **2015**, *3*, 7207.
[31] M. Rosso, T. Gobron, C. Brissot, J. N. Chazalviel, S. Lascaud, *J. Power Sources* **2001**, *97*, 804.
[32] J. Tan, J. Matz, P. Dong, J. Shen, M. Ye, *Adv. Energy Mater.* **2021**, *11*, 2100046.
[33] K. Xu, *Chem. Rev.* **2014**, *114*, 11503.
[34] N. Nitta, F. Wu, J. T. Lee, G. Yushin, *Mater. Today* **2015**, *18*, 252.
[35] K. Edström, M. Herstedt, D. P. Abraham, *J. Power Sources* **2006**, *153*, 380.
[36] M. Gauthier, T. J. Carney, A. Grimaud, L. Giordano, N. Pour, H. H. Chang, D. P. Fenning, S. F. Lux, O. Paschos, C. Bauer, F. Maglia, S. Lupart, P. Lamp, Y. Shao-Horn, *J. Phys. Chem. Lett.* **2015**, *6*, 4653.
[37] P. Verma, P. Maire, P. Novák, *Electrochim. Acta* **2010**, *55*, 6332.
[38] R. Yazami, P. Touzain, *J. Power Sources* **1983**, *9*, 365.
[39] K. Edström, T. Gustafsson, J. O. Thomas, *Electrochim. Acta* **2004**, *50*, 397.
[40] M. Winter, *Z. Phys. Chem.* **2009**, *223*, 1395.
[41] S. J. An, J. Li, C. Daniel, D. Mohanty, S. Nagpure, D. L. Wood, *Carbon* **2016**, *105*, 52.
[42] E. Peled, S. Menkin, *J. Electrochem. Soc.* **2017**, *164*, A1703.
[43] A. Wang, S. Kadam, H. Li, S. Shi, Y. Qi, *npj Comput. Mater.* **2018**, *4*, 15.
[44] D. Diddens, W. A. Appiah, Y. Mabrouk, A. Heuer, T. Vegge, A. Bhowmik, *Adv. Mater. Interfaces* **2022**, *9*, 2101734.
[45] X. Shan, Y. Zhong, L. Zhang, Y. Zhang, X. Xia, X. Wang, J. Tu, *J. Phys. Chem. C* **2021**, *125*, 19060.
[46] V. A. Agubra, J. W. Fergus, *J. Power Sources* **2014**, *268*, 153.
[47] F. A. Soto, Y. Ma, J. M. Martinez De La Hoz, J. M. Seminario, P. B. Balbuena, *Chem. Mater.* **2015**, *27*, 7990.
[48] S. K. Heiskanen, J. Kim, B. L. Lucht, *Joule* **2019**, *3*, 2322.
[49] M. Nie, D. Chalasani, D. P. Abraham, Y. Chen, A. Bose, B. L. Lucht, *J. Phys. Chem. C* **2013**, *117*, 13403.
[50] S. Malmgren, K. Ciosek, M. Hahlin, T. Gustafsson, M. Gorgoi, H. Rensmo, K. Edström, *Electrochim. Acta* **2013**, *97*, 23.
[51] D. P. Finegan, M. Scheel, J. B. Robinson, B. Tjaden, I. Hunt, T. J. Mason, J. Millichamp, M. Di Michiel, G. J. Offer, G. Hinds, D. J. L. Brett, P. R. Shearing, *Nat. Commun.* **2015**, *6*, 6924.
[52] S. Abada, G. Marlair, A. Lecocq, M. Petit, V. Sauvant-Moynot, F. Huet, *J. Power Sources* **2016**, *306*, 178.

[53] H. Maleki, G. Deng, A. Anani, J. Howard, *J. Electrochem. Soc.* **1999**, *146*, 3224.
[54] M. B. Pinson, M. Z. Bazant, *J. Electrochem. Soc.* **2013**, *160*, A243.
[55] G. G. Eshetu, H. Zhang, X. Judez, H. Adenusi, M. Armand, S. Passerini, E. Figgemeier, *Nat. Commun.* **2021**, *12*, 5459.
[56] J. Sonnefeld, *Colloid Polym. Sci.* **1995**, *273*, 932.
[57] G. V. Franks, *J. Colloid Interface Sci.* **2002**, *249*, 44.
[58] M. Kosmulski, *J. Colloid Interface Sci.* **1998**, *208*, 543.
[59] M. Porus, C. Labbez, P. Maroni, M. Borkovec, *J. Chem. Phys.* **2011**, *135*, 061101.
[60] D. J. Tobias, J. C. Hemminger, *Science* **2008**, *319*, 1197.
[61] P. Iamprasertkun, W. Hirunpinyopas, A. Keerthi, B. Wang, B. Radha, M. A. Bissett, R. A. W. Dryfe, *J. Phys. Chem. Lett.* **2019**, *10*, 617.
[62] H. Helmholtz, *Ann. Phys. Chem.* **1879**, *7*, 22.
[63] V. Bagotsky, *Fundamentals of Electrochemistry*, Wiley, Hoboken, NJ **2006**.
[64] T. Dabros, *Can. J. Chem. Eng.* **2006**, *84*, 729.
[65] M. Gouy, *J. Phys. Theor. Appl.* **1910**, *9*, 457.
[66] D. Chapman, *Philos. Mag.* **1913**, *25*, 475.
[67] O. Stern, *Z. Elektrochem.* **1924**, *30*, 508.
[68] O. Borodin, X. Ren, J. Vatamanu, A. Von Wald Cresce, J. Knap, K. Xu, *Acc. Chem. Res.* **2017**, *50*, 2886.
[69] J. Vatamanu, O. Borodin, *J. Phys. Chem. Lett.* **2017**, *8*, 4362.
[70] L. Pilon, H. Wang, A. d'Entremont, *J. Electrochem. Soc.* **2015**, *162*, A5158.
[71] O. Borodin, *Curr. Opin. Electrochem.* **2019**, *13*, 86.
[72] A. N. Dey, B. P. Sullivan, *J. Electrochem. Soc.* **1970**, *117*, 222.
[73] A. N. Dey, *Thin Solid Films* **1977**, *43*, 131.
[74] E. Peled, *J. Electrochem. Soc.* **1979**, *126*, 2047.
[75] E. Peled, *J. Power Sources* **1983**, *9*, 253.
[76] G. Nazri, R. Muller, *J. Electrochem. Soc.* **1985**, *132*, 2050.
[77] G. Nazri, R. Muller, *J. Electrochem. Soc.* **1985**, *132*, 1385.
[78] D. Aurbach, M. Daroux, P. Faguy, E. Yeager, *J. Electrochem. Soc.* **1987**, *134*, 1611.
[79] R. Fong, U. Von Sacken, J. R. Dahn, *J. Electrochem. Soc.* **1990**, *137*, 2009.
[80] K. Kanamura, H. Tamura, S. Shiraishi, Z. Takehara, *J. Electrochem. Soc.* **1995**, *142*, 340.
[81] K. Kanamura, H. Tamura, S. Shiraishi, Z. I. Takehara, *Electrochim. Acta* **1995**, *40*, 913.
[82] A. Zaban, E. Zinigrad, D. Aurbach, *J. Phys. Chem.* **1996**, *100*, 3089.
[83] E. Peled, D. Golodnitsky, G. Ardel, V. Eshkenazy, *Electrochim. Acta* **1995**, *40*, 2197.
[84] E. Peled, D. Golodnitsky, G. Ardel, *J. Electrochem. Soc.* **1997**, *144*, L208.
[85] D. Aurbach, B. Markovsky, M. D. Levi, E. Levi, A. Schechter, M. Moshkovich, Y. Cohen, *J. Power Sources* **1999**, *81–82*, 95.
[86] A. V. Cresce, S. M. Russell, D. R. Baker, K. J. Gaskell, K. Xu, *Nano Lett.* **2014**, *14*, 1405.
[87] B. C. Melot, J. M. Tarascon, *Acc. Chem. Res.* **2013**, *46*, 1226.
[88] C. Liu, Z. G. Neale, G. Cao, *Mater. Today* **2016**, *19*, 109.
[89] N. Kumar, D. J. Siegel, *J. Phys. Chem. Lett.* **2016**, *7*, 874.
[90] J. B. Goodenough, *Energy Environ. Sci.* **2014**, *7*, 14.
[91] R. Hausbrand, *J. Chem. Phys.* **2020**, *152*, 180902.
[92] P. Peljo, H. H. Girault, *Energy Environ. Sci.* **2018**, *11*, 2306.
[93] E. Endo, M. Ata, K. Tanaka, K. Sekai, *J. Electrochem. Soc.* **1998**, *145*, 3757.
[94] K. Leung, *J. Phys. Chem. C* **2013**, *117*, 1539.
[95] P. Johansson, P. Jacobsson, *J. Power Sources* **2006**, *153*, 336.
[96] S. A. Delp, O. Borodin, M. Olguin, C. G. Eisner, J. L. Allen, T. R. Jow, *Electrochim. Acta* **2016**, *209*, 498.
[97] L. Xing, O. Borodin, *Phys. Chem. Chem. Phys.* **2012**, *14*, 12838.
[98] L. Xing, X. Zheng, M. Schroeder, J. Alvarado, A. Von Wald Cresce, K. Xu, Q. Li, W. Li, *Acc. Chem. Res.* **2018**, *51*, 282.
[99] Y. Li, K. Leung, Y. Qi, *Acc. Chem. Res.* **2016**, *49*, 2363.
[100] G. V. Zhuang, H. Yang, B. Blizanac, P. N. Ross, *Electrochem. Solid-State Lett.* **2005**, *8*, A441.
[101] X. Wu, H. Li, L. Chen, X. Huang, *Solid State Ionics* **2002**, *149*, 185.
[102] S. B. Lee, S. Il Pyun, *Carbon* **2002**, *40*, 2333.
[103] K. Tasaki, S. J. Harris, *J. Phys. Chem. C* **2010**, *114*, 8076.
[104] D. Aurbach, M. D. Levi, E. Levi, A. Schechter, *J. Phys. Chem. B* **1997**, *101*, 2195.
[105] K. Tasaki, A. Goldberg, M. Winter, *Electrochim. Acta* **2011**, *56*, 10424.
[106] K. Xu, Y. Lam, S. S. Zhang, T. R. Jow, T. B. Curtis, *J. Phys. Chem. C* **2007**, *111*, 7411.
[107] D. Aurbach, A. Zaban, A. Schechter, Y. Ein-Eli, E. Zinigrad, B. Markovsky, *J. Electrochem. Soc.* **1995**, *142*, 2873.
[108] G. V. Zhuang, K. Xu, H. Yang, T. R. Jow, P. N. Ross, *J. Phys. Chem. B* **2005**, *109*, 17567.
[109] D. Aurbach, B. Markovsky, A. Shechter, Y. Ein-Eli, H. Cohen, *J. Electrochem. Soc.* **1996**, *143*, 3809.
[110] D. Aurbach, B. Markovsky, I. Weissman, E. Levi, Y. Ein-Eli, *Electrochim. Acta* **1999**, *45*, 67.
[111] P. Lu, C. Li, E. W. Schneider, S. J. Harris, *J. Phys. Chem. C* **2014**, *118*, 896.
[112] S. J. Harris, P. Lu, *J. Phys. Chem. C* **2013**, *117*, 6481.
[113] D. Zane, A. Antonini, M. Pasquali, *J. Power Sources* **2001**, *97–98*, 146.
[114] V. Agubra, J. Fergus, *Materials* **2013**, *6*, 1310.
[115] D. Bar-Tow, E. Peled, L. Burstein, *J. Electrochem. Soc.* **1999**, *146*, 824.
[116] E. Peled, D. B. Tow, A. Merson, L. Burstein, *J. New Mater. Electrochem. Syst.* **2000**, *3*, 319.
[117] M. Velický, P. S. Toth, C. R. Woods, K. S. Novoselov, R. A. W. Dryfe, *J. Phys. Chem. C* **2019**, *123*, 11677.
[118] E. Peled, D. Bar Tow, A. Merson, A. Gladkich, L. Burstein, D. Golodnitsky, *J. Power Sources* **2001**, *97–98*, 52.
[119] Y. Domi, M. Ochida, S. Tsubouchi, H. Nakagawa, T. Yamanaka, T. Doi, T. Abe, Z. Ogumi, *J. Phys. Chem. C* **2011**, *115*, 25484.
[120] S. Shiraishi, K. Kanamura, Z. I. Takehara, *Langmuir* **1997**, *13*, 3542.
[121] S.-K. Jeong, M. Inaba, T. Abe, Z. Ogumi, *J. Electrochem. Soc.* **2001**, *148*, A989.
[122] S. Tsubouchi, Y. Domi, T. Doi, M. Ochida, H. Nakagawa, T. Yamanaka, T. Abe, Z. Ogumi, *J. Electrochem. Soc.* **2012**, *159*, A1786.
[123] V. Eshkenazi, E. Peled, L. Burstein, D. Golodnitsky, *Solid State Ionics* **2004**, *170*, 83.
[124] E. Peled, D. Golodnitsky, C. Menachem, D. Bar-Tow, *J. Electrochem. Soc.* **1998**, *145*, 3482.
[125] J. O. Besenhard, M. Winter, J. Yang, W. Biberacher, *J. Power Sources* **1995**, *54*, 228.
[126] I. A. Shkrob, Y. Zhu, T. W. Marin, D. Abraham, *J. Phys. Chem. C* **2013**, *117*, 19255.
[127] I. A. Shkrob, Y. Zhu, T. W. Marin, D. Abraham, *J. Phys. Chem. C* **2013**, *117*, 19270.
[128] Y. Wang, S. Nakamura, M. Ue, P. B. Balbuena, *J. Am. Chem. Soc.* **2001**, *123*, 11708.
[129] J. M. Vollmer, L. A. Curtiss, D. R. Vissers, K. Amine, *J. Electrochem. Soc.* **2004**, *151*, A178.
[130] R. L. McCreery, *Chem. Rev.* **2008**, *108*, 2646.
[131] C. E. Banks, T. J. Davies, G. G. Wildgoose, R. G. Compton, *Chem. Commun.* **2005**, 829.
[132] Y. Chen, M. Huo, L. Song, Z. Sun, *J. Phys. Chem. C* **2011**, *115*, 7044.
[133] S. Shi, P. Lu, Z. Liu, Y. Qi, L. G. Hector, H. Li, S. J. Harris, *J. Am. Chem. Soc.* **2012**, *134*, 15476.
[134] R. Guo, B. M. Gallant, *Chem. Mater.* **2020**, *32*, 5525.
[135] S. Lorger, R. Usiskin, J. Maier, *J. Electrochem. Soc.* **2019**, *166*, A2215.
[136] J. S. Lowe, D. J. Siegel, *ACS Appl. Mater. Interfaces* **2020**, *12*, 46015.

[137] K. Xu, G. V. Zhuang, J. L. Allen, U. Lee, S. S. Zhang, P. N. Ross, T. R. Jow, *J. Phys. Chem. B* **2006**, *110*, 7708.
[138] J. S. Gnanaraj, R. W. Thompson, S. N. Iaconatti, J. F. Dicarlo, K. M. Abraham, *Electrochem. Solid-State Lett.* **2005**, *8*, A128.
[139] K. L. Browning, L. Baggetto, R. R. Unocic, N. J. Dudney, G. M. Veith, *J. Power Sources* **2013**, *239*, 341.
[140] G. V. Zhuang, P. N. Ross, *Electrochem. Solid-State Lett.* **2003**, *6*, A136.
[141] L. Chen, J. Shu, Y. Huang, Z. Shi, H. Luo, Z. Liu, C. Shen, *Appl. Surf. Sci.* **2022**, *598*, 153740.
[142] C. Fringant, A. Tranchant, R. Messina, *Electrochim. Acta* **1995**, *40*, 513.
[143] D. Lu, M. Xu, L. Zhou, A. Garsuch, B. L. Lucht, *J. Electrochem. Soc.* **2013**, *160*, A3138.
[144] T. Li, L. Xing, W. Li, Y. Wang, M. Xu, F. Gu, S. Hu, *J. Power Sources* **2013**, *244*, 668.
[145] H. Zhang, G. Guo, H. Adenusi, B. Qin, H. Li, S. Passerini, W. Huang, *Mater. Today* **2022**, *53*, 162.
[146] A. J. Loebl, C. J. Oldham, C. K. Devine, B. Gong, S. E. Atanasov, G. N. Parsons, P. S. Fedkiw, *J. Electrochem. Soc.* **2013**, *160*, A1971.
[147] P. Bernardo, J. M. Le Meins, L. Vidal, J. Dentzer, R. Gadiou, W. Märkle, P. Novák, M. E. Spahr, C. Vix-Guterl, *Carbon* **2015**, *91*, 458.
[148] M. Park, X. Zhang, M. Chung, G. B. Less, A. M. Sastry, *J. Power Sources* **2010**, *195*, 7904.
[149] J. Yan, J. Zhang, Y. C. Su, X. G. Zhang, B. J. Xia, *Electrochim. Acta* **2010**, *55*, 1785.
[150] R. Dedryvère, H. Martinez, S. Leroy, D. Lemordant, F. Bonhomme, P. Biensan, D. Gonbeau, *J. Power Sources* **2007**, *174*, 462.
[151] C. Huang, S. Zhuang, F. Tu, *J. Electrochem. Soc.* **2013**, *160*, A376.
[152] G.-C. Chung, H.-J. Kim, S.-I. Yu, S.-H. Jun, J. Choi, M.-H. Kim, *J. Electrochem. Soc.* **2000**, *147*, 4391.
[153] Y. Okamoto, *J. Electrochem. Soc.* **2013**, *160*, A404.
[154] D. Aurbach, M. Moshkovich, *J. Electrochem. Soc.* **1998**, *145*, 2629.
[155] K. Leung, *Chem. Phys. Lett.* **2013**, *568–569*, 1.
[156] J. Zhang, J. Yang, L. Yang, H. Lu, H. Liu, B. Zheng, *Mater. Adv.* **2021**, *2*, 1747.
[157] T. Li, P. B. Balbuena, *Chem. Phys. Lett.* **2000**, *317*, 421.
[158] S. Leroy, H. Martinez, R. Dedryvère, D. Lemordant, D. Gonbeau, *Appl. Surf. Sci.* **2007**, *253*, 4895.
[159] F. Joho, P. Novák, *Electrochim. Acta* **2000**, *45*, 3589.
[160] C. L. Campion, W. Li, W. B. Euler, B. L. Lucht, B. Ravdel, J. F. DiCarlo, R. Gitzendanner, K. M. Abraham, *Electrochem. Solid-State Lett.* **2004**, *7*, A194.
[161] A. Schechter, D. Aurbach, H. Cohen, *Langmuir* **1999**, *15*, 3334.
[162] M. Broussely, P. Biensan, F. Bonhomme, P. Blanchard, S. Herreyre, K. Nechev, R. J. Staniewicz, *J. Power Sources* **2005**, *146*, 90.
[163] H. Yamada, Y. Watanabe, I. Moriguchi, T. Kudo, *Solid State Ionics* **2008**, *179*, 1706.
[164] P. Novák, F. Joho, M. Lanz, B. Rykart, J. C. Panitz, D. Alliata, R. Kötz, O. Haas, *J. Power Sources* **2001**, *97–98*, 39.
[165] M. Stich, M. Göttlinger, M. Kurniawan, U. Schmidt, A. Bund, *J. Phys. Chem. C* **2018**, *122*, 8836.
[166] T. Yoshida, M. Takahashi, S. Morikawa, C. Ihara, H. Katsukawa, T. Shiratsuchi, J. Yamaki, *J. Electrochem. Soc.* **2006**, *153*, A576.
[167] B. T. Young, D. R. Heskett, C. C. Nguyen, M. Nie, J. C. Woicik, B. L. Lucht, *ACS Appl. Mater. Interfaces* **2015**, *7*, 20004.
[168] B. Horstmann, J. Shi, R. Amine, M. Werres, X. He, H. Jia, F. Hausen, I. Cekic-Laskovic, S. Wiemers-Meyer, J. Lopez, D. Galvez-Aranda, F. Baakes, D. Bresser, C. C. Su, Y. Xu, W. Xu, P. Jakes, R. A. Eichel, E. Figgemeier, U. Krewer, J. M. Seminario, P. B. Balbuena, C. Wang, S. Passerini, Y. Shao-Horn, M. Winter, K. Amine, R. Kostecki, A. Latz, *Energy Environ. Sci.* **2021**, *14*, 5289.
[169] X. Liu, A. Mariani, T. Diemant, M. E. Di Pietro, X. Dong, M. Kuenzel, A. Mele, S. Passerini, *Adv. Energy Mater.* **2022**, *12*, 2200862.
[170] Y. Yamada, J. Wang, S. Ko, E. Watanabe, A. Yamada, *Nat. Energy* **2019**, *4*, 269.
[171] L. Wang, A. Menakath, F. Han, Y. Wang, P. Y. Zavalij, K. J. Gaskell, O. Borodin, D. Iuga, S. P. Brown, C. Wang, K. Xu, B. W. Eichhorn, *Nat. Chem.* **2019**, *11*, 789.
[172] W. Xu, J. Wang, F. Ding, X. Chen, E. Nasybulin, Y. Zhang, J. G. Zhang, *Energy Environ. Sci.* **2014**, *7*, 513.
[173] J. G. Zhang, W. Xu, J. Xiao, X. Cao, J. Liu, *Chem. Rev.* **2020**, *120*, 13312.
[174] K. Deng, D. Han, S. Ren, S. Wang, M. Xiao, Y. Meng, *J. Mater. Chem. A* **2019**, *7*, 13113.
[175] Q. Zhao, S. Stalin, L. A. Archer, *Joule* **2021**, *5*, 1119.
[176] G. G. Eshetu, X. Judez, C. Li, M. Martinez-Ibañez, I. Gracia, O. Bondarchuk, J. Carrasco, L. M. Rodriguez-Martinez, H. Zhang, M. Armand, *J. Am. Chem. Soc.* **2018**, *140*, 9921.
[177] D. Aurbach, *J. Power Sources* **2000**, *89*, 206.
[178] K. Leung, F. Soto, K. Hankins, P. B. Balbuena, K. L. Harrison, *J. Phys. Chem. C* **2016**, *120*, 6302.
[179] S. Jiao, J. Zheng, Q. Li, X. Li, M. H. Engelhard, R. Cao, J. G. Zhang, W. Xu, *Joule* **2018**, *2*, 110.
[180] F. Shi, A. Pei, D. T. Boyle, J. Xie, X. Yu, X. Zhang, Y. Cui, *Proc. Natl. Acad. Sci. U. S. A.* **2018**, *115*, 8529.
[181] K. Zhang, G. H. Lee, M. Park, W. Li, Y. M. Kang, *Adv. Energy Mater.* **2016**, *6*, 1600811.
[182] F. Sun, L. Zielke, H. Markötter, A. Hilger, D. Zhou, R. Moroni, R. Zengerle, S. Thiele, J. Banhart, I. Manke, *ACS Nano* **2016**, *10*, 7990.
[183] F. Orsini, A. Du Pasquier, B. Beaudouin, J. M. Tarascon, M. Trentin, N. Langenhuizen, E. De Beer, P. Notten, *J. Power Sources* **1999**, *81–82*, 918.
[184] P. Bai, J. Li, F. R. Brushett, M. Z. Bazant, *Energy Environ. Sci.* **2016**, *9*, 3221.
[185] H. Ota, T. Akai, H. Namita, S. Yamaguchi, M. Nomura, *J. Power Sources* **2003**, *119–121*, 567.
[186] G. Gachot, S. Grugeon, M. Armand, S. Pilard, P. Guenot, J. M. Tarascon, S. Laruelle, *J. Power Sources* **2008**, *178*, 409.
[187] Z. Zhang, K. Smith, R. Jervis, P. R. Shearing, T. S. Miller, D. J. L. Brett, *ACS Appl. Mater. Interfaces* **2020**, *12*, 35132.
[188] D. Aurbach, Y. Cohen, *J. Electrochem. Soc.* **1996**, *143*, 3525.
[189] F. P. Campana, H. Buqa, P. Novák, R. Kötz, H. Siegenthaler, *Electrochem. Commun.* **2008**, *10*, 1590.
[190] M. Inaba, Z. Siroma, A. Funabiki, Z. Ogumi, T. Abe, Y. Mizutani, M. Asano, *Langmuir* **1996**, *12*, 1535.
[191] M. Inaba, Y. Kawatate, A. Funabiki, S. K. Jeong, T. Abe, Z. Ogumi, *Electrochim. Acta* **1999**, *45*, 99.
[192] A. Kominato, E. Yasukawa, N. Sato, T. Ijuuin, H. Asahina, S. Mori, *J. Power Sources* **1997**, *68*, 471.
[193] M. Dollé, L. Sannier, B. Beaudoin, M. Trentin, J. M. Tarascon, *Electrochem. Solid-State Lett.* **2002**, *5*, A286.
[194] R. L. Sacci, N. J. Dudney, K. L. More, L. R. Parent, I. Arslan, N. D. Browning, R. R. Unocic, *Chem. Commun.* **2014**, *50*, 2104.
[195] R. L. Sacci, J. M. Black, N. Balke, N. J. Dudney, K. L. More, R. R. Unocic, *Nano Lett.* **2015**, *15*, 2011.
[196] S. Jurng, Z. L. Brown, J. Kim, B. L. Lucht, *Energy Environ. Sci.* **2018**, *11*, 2600.
[197] D. Aurbach, K. Gamolsky, B. Markovsky, G. Salitra, Y. Gofer, U. Heider, R. Oesten, M. Schmidt, *J. Electrochem. Soc.* **2000**, *147*, 1322.
[198] X. Zhang, R. Kostecki, T. J. Richardson, J. K. Pugh, P. N. Ross, *J. Electrochem. Soc.* **2001**, *148*, A1341.
[199] F. Shi, P. N. Ross, H. Zhao, G. Liu, G. A. Somorjai, K. Komvopoulos, *J. Am. Chem. Soc.* **2015**, *137*, 3181.
[200] S. S. Zhang, K. Xu, T. R. Jow, *Electrochim. Acta* **2004**, *49*, 1057.
[201] J. Nanda, G. Yang, T. Hou, D. N. Voylov, X. Li, R. E. Ruther, M. Naguib, K. Persson, G. M. Veith, A. P. Sokolov, *Joule* **2019**, *3*, 2001.

[202] A. Gajan, C. Lecourt, B. E. Torres Bautista, L. Fillaud, J. Demeaux, I. T. Lucas, *ACS Energy Lett.* **2021**, *6*, 1757.
[203] N. Mozhzhukhina, E. Flores, R. Lundström, V. Nyström, P. G. Kitz, K. Edström, E. J. Berg, *J. Phys. Chem. Lett.* **2020**, *11*, 4119.
[204] A. M. Andersson, K. Edström, *J. Electrochem. Soc.* **2001**, *148*, A1100.
[205] B. M. Meyer, N. Leifer, S. Sakamoto, S. G. Greenbaum, C. P. Grey, *Electrochem. Solid-State Lett.* **2005**, *8*, A145.
[206] L. Gireaud, S. Grugeon, S. Laruelle, S. Pilard, J.-M. Tarascon, *J. Electrochem. Soc.* **2005**, *152*, A850.
[207] N. Leifer, M. C. Smart, G. K. S. Prakash, L. Gonzalez, L. Sanchez, K. A. Smith, P. Bhalla, C. P. Grey, S. G. Greenbaum, *J. Electrochem. Soc.* **2011**, *158*, A471.
[208] C. Marino, A. Darwiche, N. Dupré, H. A. Wilhelm, B. Lestriez, H. Martinez, R. Dedryvère, W. Zhang, F. Ghamouss, D. Lemordant, L. Monconduit, *J. Phys. Chem. C* **2013**, *117*, 19302.
[209] Y. S. Meng, M. E. Arroyo-De Dompablo, *Energy Environ. Sci.* **2009**, *2*, 589.
[210] A. A. Franco, *RSC Adv.* **2013**, *3*, 13027.
[211] D. Grazioli, M. Magri, A. Salvadori, *Comput. Mech.* **2016**, *58*, 889.
[212] A. Urban, D. H. Seo, G. Ceder, *npj Comput. Mater.* **2016**, *2*, 16002.
[213] A. A. Franco, A. Rucci, D. Brandell, C. Frayret, M. Gaberscek, P. Jankowski, P. Johansson, *Chem. Rev.* **2019**, *119*, 4569.
[214] N. Takenaka, Y. Suzuki, H. Sakai, M. Nagaoka, *J. Phys. Chem. C* **2014**, *118*, 10874.
[215] G. Ramos-Sanchez, F. A. Soto, J. M. Martinez De La Hoz, Z. Liu, P. P. Mukherjee, F. El-Mellouhi, J. M. Seminario, P. B. Balbuena, *J. Electrochem. Energy Convers. Storage* **2016**, *13*, 031002.
[216] O. Borodin, M. Olguin, C. E. Spear, K. W. Leiter, J. Knap, *Nanotechnology* **2015**, *26*, 354003.
[217] E. R. Fadel, F. Faglioni, G. Samsonidze, N. Molinari, B. V. Merinov, W. A. Goddard, J. C. Grossman, J. P. Mailoa, B. Kozinsky, *Nat. Commun.* **2019**, *10*, 3360.
[218] O. Borodin, W. Behl, T. R. Jow, *J. Phys. Chem. C* **2013**, *117*, 8661.
[219] N. von Aspern, M. Grünebaum, D. Diddens, T. Pollard, C. Wölke, O. Borodin, M. Winter, I. Cekic-Laskovic, *J. Power Sources* **2020**, *461*, 228159.
[220] A. Von Wald Cresce, M. Gobet, O. Borodin, J. Peng, S. M. Russell, E. Wikner, A. Fu, L. Hu, H. S. Lee, Z. Zhang, X. Q. Yang, S. Greenbaum, K. Amine, K. Xu, *J. Phys. Chem. C* **2015**, *119*, 27255.
[221] K. Leung, C. M. Tenney, *J. Phys. Chem. C* **2013**, *117*, 24224.
[222] K. Leung, J. L. Budzien, *Phys. Chem. Chem. Phys.* **2010**, *12*, 6583.
[223] D. Bedrov, G. D. Smith, A. C. T. Van Duin, *J. Phys. Chem. A* **2012**, *116*, 2978.
[224] L. Xing, O. Borodin, G. D. Smith, W. Li, *J. Phys. Chem. A* **2011**, *115*, 13896.
[225] Y. Okuno, K. Ushirogata, K. Sodeyama, Y. Tateyama, *Phys. Chem. Chem. Phys.* **2016**, *18*, 8643.
[226] W. I. Choi, M. S. Park, Y. Shim, D. Y. Kim, Y. S. Kang, H. S. Lee, M. Koh, *Phys. Chem. Chem. Phys.* **2019**, *21*, 5489.
[227] K. Ushirogata, K. Sodeyama, Y. Okuno, Y. Tateyama, *J. Am. Chem. Soc.* **2013**, *135*, 11967.
[228] J. Yu, P. B. Balbuena, J. Budzien, K. Leung, *J. Electrochem. Soc.* **2011**, *158*, A400.
[229] O. Borodin, M. Olguin, P. Ganesh, P. R. C. Kent, J. L. Allen, W. A. Henderson, *Phys. Chem. Chem. Phys.* **2016**, *18*, 164.
[230] K. Tasaki, *J. Phys. Chem. B* **2005**, *109*, 2920.
[231] O. Borodin, G. D. Smith, *J. Phys. Chem. B* **2009**, *113*, 1763.
[232] O. Borodin, S.-D. Han, J. S. Daubert, D. M. Seo, S.-H. Yun, W. A. Henderson, *J. Electrochem. Soc.* **2015**, *162*, A501.
[233] O. Borodin, *J. Phys. Chem. B* **2009**, *113*, 11463.
[234] A. C. T. Van Duin, S. Dasgupta, F. Lorant, W. A. Goddard, *J. Phys. Chem. A* **2001**, *105*, 9396.
[235] S. P. Kim, A. C. T. V. Duin, V. B. Shenoy, *J. Power Sources* **2011**, *196*, 8590.
[236] M. M. Islam, G. Kolesov, T. Verstraelen, E. Kaxiras, A. C. T. Van Duin, *J. Chem. Theory Comput.* **2016**, *12*, 3463.
[237] M. M. Islam, A. C. T. Van Duin, *J. Phys. Chem. C* **2016**, *120*, 27128.
[238] M. J. Hossain, G. Pawar, B. Liaw, K. L. Gering, E. J. Dufek, A. C. T. Van Duin, *J. Chem. Phys.* **2020**, 152, 184301.
[239] K. A. Willets, R. P. Van Duyne, *Annu. Rev. Phys. Chem.* **2007**, *58*, 267.
[240] T. Liu, L. Lin, X. Bi, L. Tian, K. Yang, J. Liu, M. Li, Z. Chen, J. Lu, K. Amine, K. Xu, F. Pan, *Nat. Nanotechnol.* **2019**, *14*, 50.
[241] Y. Zhou, M. Su, X. Yu, Y. Zhang, J. G. Wang, X. Ren, R. Cao, W. Xu, D. R. Baer, Y. Du, O. Borodin, Y. Wang, X. L. Wang, K. Xu, Z. Xu, C. Wang, Z. Zhu, *Nat. Nanotechnol.* **2020**, *15*, 224.
[242] H. Zhu, J. A. Russell, Z. Fang, P. Barnes, L. Li, C. M. Efaw, A. Muenzer, J. May, K. Hamal, I. F. Cheng, P. H. Davis, E. J. Dufek, H. Xiong, *Small* **2021**, *17*, 2105292.
[243] S. Yuan, S. Weng, F. Wang, X. Dong, Y. Wang, Z. Wang, C. Shen, J. L. Bao, X. Wang, Y. Xia, *Nano Energy* **2021**, *83*, 105847.
[244] X. Wang, M. Zhang, J. Alvarado, S. Wang, M. Sina, B. Lu, J. Bouwer, W. Xu, J. Xiao, J. G. Zhang, J. Liu, Y. S. Meng, *Nano Lett.* **2017**, *17*, 7606.
[245] L. Mai, M. Yan, Y. Zhao, *Nature* **2017**, *546*, 469.
[246] D. T. Boyle, X. Kong, A. Pei, P. E. Rudnicki, F. Shi, W. Huang, Z. Bao, J. Qin, Y. Cui, *ACS Energy Lett.* **2020**, *5*, 701.
[247] T. Morimoto, M. Nagai, Y. Minowa, M. Ashida, Y. Yokotani, Y. Okuyama, Y. Kani, *Nat. Commun.* **2019**, *10*, 2662.
[248] D. Krotkov, D. Schneier, S. Menkin, Y. Horowitz, E. Peled, D. Golodnitsky, S. Fleischer, *Batteries Supercaps* **2022**, *5*, 202100183.
[249] W. J. Zhang, *J. Power Sources* **2011**, *196*, 13.
[250] J. Saint, M. Morcrette, D. Larcher, L. Laffont, S. Beattie, J. P. Pérès, D. Talaga, M. Couzi, J. M. Tarascon, *Adv. Funct. Mater.* **2007**, *17*, 1765.
[251] C. M. Park, H. J. Sohn, *Electrochim. Acta* **2009**, *54*, 6367.
[252] X. He, D. Bresser, S. Passerini, F. Baakes, U. Krewer, J. Lopez, C. T. Mallia, Y. Shao-Horn, I. Cekic-Laskovic, S. Wiemers-Meyer, F. A. Soto, V. Ponce, J. M. Seminario, P. B. Balbuena, H. Jia, W. Xu, Y. Xu, C. Wang, B. Horstmann, R. Amine, C. C. Su, J. Shi, K. Amine, M. Winter, A. Latz, R. Kostecki, *Nat. Rev. Mater.* **2021**, *6*, 1036.
[253] L. A. Riley, A. S. Cavanagh, S. M. George, S. H. Lee, A. C. Dillon, *Electrochem. Solid-State Lett.* **2011**, *14*, 2010.
[254] Y. S. Jung, A. S. Cavanagh, L. A. Riley, S. H. Kang, A. C. Dillon, M. D. Groner, S. M. George, S. H. Lee, *Adv. Mater.* **2010**, *22*, 2172.
[255] L. Han, C. Te Hsieh, B. Chandra Mallick, J. Li, Y. Ashraf Gandomi, *Nanoscale Adv.* **2021**, *3*, 2728.
[256] Y. Zhao, M. Amirmaleki, Q. Sun, C. Zhao, A. Codirenzi, L. V. Goncharova, C. Wang, K. Adair, X. Li, X. Yang, F. Zhao, R. Li, T. Filleter, M. Cai, X. Sun, *Matter* **2019**, *1*, 1215.
[257] X. Meng, *Energy Storage Mater.* **2020**, *30*, 296.
[258] A. C. Kozen, C. F. Lin, A. J. Pearse, M. A. Schroeder, X. Han, L. Hu, S. B. Lee, G. W. Rubloff, M. Noked, *ACS Nano* **2015**, *9*, 5884.
[259] R. Xu, C. Yan, J. Q. Huang, *Trends Chem.* **2021**, *3*, 5.
[260] A. Bhowmik, I. E. Castelli, J. M. Garcia-Lastra, P. B. Jørgensen, O. Winther, T. Vegge, *Energy Storage Mater.* **2019**, *21*, 446.
[261] F. Wang, O. Borodin, M. S. Ding, M. Gobet, J. Vatamanu, X. Fan, T. Gao, N. Edison, Y. Liang, W. Sun, S. Greenbaum, K. Xu, C. Wang, *Joule* **2018**, *2*, 927.
[262] C. Yang, J. Chen, T. Qing, X. Fan, W. Sun, A. von Cresce, M. S. Ding, O. Borodin, J. Vatamanu, M. A. Schroeder, N. Eidson, C. Wang, K. Xu, *Joule* **2017**, *1*, 122.
[263] C. Yan, H. R. Li, X. Chen, X. Q. Zhang, X. B. Cheng, R. Xu, J. Q. Huang, Q. Zhang, *J. Am. Chem. Soc.* **2019**, *141*, 9422.
[264] X. Zheng, F. Wang, C. Y. Yam, Y. Mo, G. Chen, *Phys. Rev. B: Condens. Matter Mater. Phys.* **2007**, *75*, 195127.
[265] Z. Xu, Y. Zhou, C. Y. Yam, L. Groß, A. De Sio, T. Frauenheim, C. Lienau, G. Chen, *Sci. Adv.* **2021**, *7*, eabf7672.

[266] Z. Xu, Y. Zhou, L. Groß, A. De Sio, C. Y. Yam, C. Lienau, T. Frauenheim, G. H. Chen, *Nano Lett.* **2019**, *19*, 8630.
[267] L. Chen, Y. Zhang, G. Chen, I. Franco, *Nat. Commun.* **2018**, *9*, 2070.
[268] G. Li, C. W. Monroe, *Annu. Rev. Chem. Biomol. Eng.* **2020**, *11*, 277.
[269] J. Fish, G. J. Wagner, S. Keten, *Nat. Mater.* **2021**, *20*, 774.
[270] V. L. Deringer, M. A. Caro, G. Csányi, *Adv. Mater.* **2019**, *31*, 1902765.
[271] O. T. Unke, S. Chmiela, H. E. Sauceda, M. Gastegger, I. Poltavsky, K. T. Schütt, A. Tkatchenko, K. R. Müller, *Chem. Rev.* **2021**, *121*, 10142.
[272] G. Imbalzano, A. Anelli, D. Giofré, S. Klees, J. Behler, M. Ceriotti, *J. Chem. Phys.* **2018**, *148*, 241730.
[273] Y. Zhou, J. Wu, S. Chen, G. H. Chen, *J. Phys. Chem. Lett.* **2019**, *10*, 7264.
[274] J. Behler, M. Parrinello, *Phys. Rev. Lett.* **2007**, *98*, 146401.
[275] K. T. Schütt, H. E. Sauceda, P. J. Kindermans, A. Tkatchenko, K. R. Müller, *J. Chem. Phys.* **2018**, *148*, 241722.
[276] J. Wang, D. Zhang, R. Xu, C. Yam, G. Chen, X. Zheng, *J. Phys. Chem. A* **2022**, *126*, 970.
[277] Z. Ahmad, T. Xie, C. Maheshwari, J. C. Grossman, V. Viswanathan, *ACS Cent. Sci.* **2018**, *4*, 996.
[278] Q. Sun, Y. Xiang, Y. Liu, L. Xu, T. Leng, Y. Ye, A. Fortunelli, W. A. Goddard, T. Cheng, *J. Phys. Chem. Lett.* **2022**, *13*, 8047.
[279] X. Zheng, L. H. Hu, X. J. Wang, G. H. Chen, *Chem. Phys. Lett.* **2004**, *390*, 186.
[280] L. H. Hu, X. J. Wang, L. H. Wong, G. H. Chen, *J. Chem. Phys.* **2003**, *119*, 11501.
[281] K. V. Tian, B. Yang, Y. Z. Yue, D. T. Bowron, J. Mayers, R. S. Donnan, C. Dobo-Nagy, J. W. Nicholson, D. C. Fang, A. L. Greer, G. A. Chass, G. N. Greaves, *Nat. Commun.* **2015**, *6*, 8631.
[282] K. V. Tian, G. Festa, L. Szentmiklósi, B. Maróti, L. Arcidiacono, G. Laganà, C. Andreani, S. Licoccia, R. Senesi, P. Cozza, *J. Anal. At. Spectrom.* **2017**, *32*, 1420.
[283] D. Atkins, E. Capria, K. Edström, T. Famprikis, A. Grimaud, Q. Jacquet, M. Johnson, A. Matic, P. Norby, H. Reichert, J. P. Rueff, C. Villevieille, M. Wagemaker, S. Lyonnard, *Adv. Energy Mater.* **2022**, *12*, 2102694.
[284] C. A. Bridges, X. G. Sun, J. Zhao, M. P. Paranthaman, S. Dai, *J. Phys. Chem. C* **2012**, *116*, 7701.
[285] E. Zhao, Z. G. Zhang, X. Li, L. He, X. Yu, H. Li, F. Wang, *Chin. Phys. B* **2020**, *29*, 018201.
[286] R. L. Sacci, J. L. Baniuelos, G. M. Veith, K. C. Littrell, Y. Q. Cheng, C. U. Wildgruber, L. L. Jones, A. J. Ramirez-Cuesta, G. Rother, N. J. Dudney, *J. Phys. Chem. C* **2015**, *119*, 9816.
[287] C. von Lüders, V. Zinth, S. V. Erhard, P. J. Osswald, M. Hofmann, R. Gilles, A. Jossen, *J. Power Sources* **2017**, *342*, 17.
[288] V. Zinth, C. Von Lüders, M. Hofmann, J. Hattendorff, I. Buchberger, S. Erhard, J. Rebelo-Kornmeier, A. Jossen, R. Gilles, *J. Power Sources* **2014**, *271*, 152.
[289] T. M. Fears, M. Doucet, J. F. Browning, J. K. S. Baldwin, J. G. Winiarz, H. Kaiser, H. Taub, R. L. Sacci, G. M. Veith, *Phys. Chem. Chem. Phys.* **2016**, *18*, 13927.
[290] M. H. Wood, S. M. Clark, *Metals* **2017**, *7*, 304.
[291] G. M. Veith, M. Doucet, J. K. Baldwin, R. L. Sacci, T. M. Fears, Y. Q. Wang, J. F. Browning, *J. Phys. Chem. C* **2015**, *119*, 20339.
[292] H. Kawaura, M. Harada, Y. Kondo, Y. Suganuma, N. Takahashi, J. Sugiyawa, Y. Seno, N. L. Yamada, *ACS Appl. Mater. Interfaces* **2016**, *8*, 9540.
[293] M. Steinhauer, M. Stich, M. Kurniawan, B. K. Seidlhofer, M. Trapp, A. Bund, N. Wagner, K. A. Friedrich, *ACS Appl. Mater. Interfaces* **2017**, *9*, 35794.
[294] G. M. Veith, M. Doucet, R. L. Sacci, B. Vacaliuc, J. K. Baldwin, J. F. Browning, *Sci. Rep.* **2017**, *7*, 6326.
[295] F. V. Song, B. Yang, D. Di Tommaso, R. S. Donnan, G. A. Chass, R. Y. Yada, D. H. Farrar, K. V. Tian, *Mater. Adv.* **2022**, *3*, 4982.
[296] Y. Z. Li, Y. B. Li, A. Pei, K. Yan, Y. M. Sun, C. L. Wu, L. M. Joubert, R. Chin, A. L. Koh, Y. Yu, J. Perrino, B. Butz, S. Chu, Y. Cui, *Science* **2017**, *358*, 506.
[297] Y. Liu, Y. K. Tzeng, D. Lin, A. Pei, H. Lu, N. A. Melosh, Z. X. Shen, S. Chu, Y. Cui, *Joule* **2018**, *2*, 1595.

Henry Adenusi completed his Ph.D. at Sapienza University of Rome; he was awarded the "Vito Volterra" International Fellowship. Currently, he is a postdoctoral fellow at the Hong Kong Quantum AI Lab, joint center of The University of Hong (HKU) and the California Institute of Technology (Caltech) working on the AI and quantum mechanical simulation platform for next generation materials discovery. Research focus is on merging computational simulations with electrochemistry experiments and AI technologies (machine learning) for battery materials.

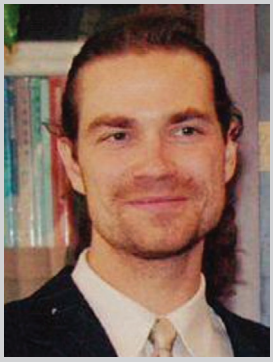

Gregory A. Chass is a reader in Computational Chemistry at the Queen Mary University of London, with adjunct professorship at McMaster University and the University of Hong Kong. His research focus and expertise lie in the computational design of experimental (neutron scattering, muon-spin resonance) characterization and optimization of novel homogeneous catalysts, cement composites, and bioactive compounds. Additional focus involves tracking of radical-scavenging proficiency in natural anti-oxidants. Fundamental methodology development involves entropy partitioning to accurately quantify free-energy of solvation and translational entropy in the condensed phase, in addition to evolving molecular-cluster approaches to computing amorphous materials and chemical transformations in solution.

Stefano Passerini is a professor at the Chemistry Department of Sapienza University of Rome. Formerly a professor at the Karlsruhe Institute of Technology, Helmholtz Institute Ulm (Germany) and the University of Muenster (Germany), he co-founded the MEET battery research center. His research focuses on the basic understanding and development of materials for high-energy batteries and supercapacitors, with the goal to create sustainable energy storage systems from environmentally friendly and available materials and processes. He is an internationally recognized pioneer in the field of ionic liquids and the development of alkali-ion batteries.

Kun V. Tian (田坤) is a senior researcher at Sapienza University of Rome, associated with McMaster University and the University of British Columbia. She applies neutron and THz spectroscopy, complemented by conventional spectroscopy, computer simulations, and bulk mechanical tests to the understanding of micro-, meso-, and macro-scale properties of materials, systems, and processes, including but not limited to functional biomaterials, cement and concrete, energy storage systems, CO_2 capture and utilization, mineralization, and agro-industrial waste utilization. Her research activities encompass basic and applied research as well as experimental development of relevant industrial processes.

Guanhua Chen is a professor of Chemistry at the University of Hong Kong. He received his Ph.D. degree in Physics in 1992 under the supervision of Prof. William Goddard III at the California Institute of Technology. He joined the University of Hong Kong in 1996 and was the head of the department of Chemistry from 2010 to 2016. He is a Fellow of the American Physical Society and a Fellow of the Royal Society of Chemistry, and the recipient of the Croucher Senior Researcher Award in 2016 and the National Natural Science Award in 2008.